Received: 29 September 2020 | Revised: 10 March 2021 | Accepted: 12 March 2021

DOI: 10.1002/nme.6676

RESEARCH ARTICLE

WILEY

Robust geometry and topology optimization of plane frames using order statistics and force density method with global stability constraint

Wei Shen[1] | **Makoto Ohsaki**[1] | **Makoto Yamakawa**[2]

[1]Department of Architecture and Architectural Engineering, Graduate School of Engineering, Kyoto University, Kyoto, Japan

[2]Department of Architecture, Tokyo University of Science, Tokyo, Japan

Correspondence
Wei Shen, Department of Architecture and Architectural Engineering, Graduate School of Engineering, Kyoto University, Kyoto-Daigaku Katsura, Nishikyo, Kyoto 615-8540, Japan.
Email: shen.wei.28a@st.kyoto-u.ac.jp

Funding information
China Scholarship Council, Grant/Award Number: 201806050114

Abstract

This paper presents a worst case approach for robust geometry and topology optimization of plane frames with global stability constraint. Uncertainty is assumed to exist in the nodal locations and cross-sectional areas, and the worst values of the objective and stability constraint functions are relaxed to the quantile structural responses represented by the order statistics with given robustness and confidence levels. In order to alleviate the difficulty caused by melting nodes to some extent, the force density method is applied to an auxiliary truss model for geometry optimization of the frame, and the closely spaced nodes are merged. A method is presented for generating correlated imperfections for the nodal locations along each member, and a penalization approach is proposed for geometrical stiffness matrix to exclude superficial local buckling. It is demonstrated in the numerical examples that the result of robust optimization obtained by the proposed method is less sensitive to the uncertainty, and the stability constraint is also satisfied under uncertainty with the specified robustness and confidence levels.

KEYWORDS

force density method, order statistics, plane frame, robust optimization, stability constraint

1 | INTRODUCTION

Geometry and topology optimization of skeletal structures has been extensively studied since the pioneering work by Maxwell and Michell, and significant effort has been made in the past few decades to the corresponding development of mathematical formulations, numerical methods, and optimization algorithms. Readers interested in this field may refer to the comprehensive review articles[1,2] and text books[3,4] to obtain a general understanding.

Instead of the well-established ground structure method where the optimization result is obtained by removing the unnecessary members from the set of potential connections of nodes and members with fixed locations,[5] geometry and topology optimization may start from a sparse initial structure because the adjustment of nodal locations can usually lead to an effective improvement of the objective value.[6] However, one of the main difficulties in geometry optimization is the existence of melting (coalescent) nodes if the nodes are allowed to move in a wide range, resulting in a singular stiffness matrix.[7] Ohsaki[8] modeled a regular grid truss as a frame with beam elements and adjusted the stiffness of a short member using a Sigmoid function. Wang et al.[9,10] proposed a node shift method for truss shape optimization where the intervals of node shift are controlled not to cause a large variation in stiffness matrix, restricting the moving ranges of the nodes.

To alleviate the difficulty caused by melting nodes, Ohsaki and Hayashi[11] and Hayashi and Ohsaki[12] reformulated the objective and constraint functions in truss optimization problem using force density method (FDM). Shen and Ohsaki[13] extended this method to frame structures by introducing an auxiliary pin-jointed truss or cable-net structure.

Since it is well known that such optimization process often converges toward a structure which lacks sufficient stability, considerable efforts are also dedicated to including stability constraint in the problem formulation.[14-16] Among all the different phenomena covered by stability theory, global instability (also called global buckling or linear buckling) is widely used to consider instability problem into structural optimization because it does not require detailed nonlinear stability information about the structure which is usually not available at the early stage of design.[17] Indeed, the nonlinear buckling load factor can be obtained by scaling the linear buckling load factor, which works well for many real-world structures and is acceptable to account for structural stability.[18] Ohsaki et al.[19] recast the optimization problem with global stability constraint as a sequential semidefinite programming for truss structures; Guo et al.[20,21] extended the relaxation method to handle the unstable phenomenon which happens when the cross-sectional area approaches the small lower bound. Descamps and Coelho[22] used force density as an intermediate variable in the formulation of compliance minimization problem, and avoided the nodal instability by applying the nominal force method to simulate the geometric imperfection. Furthermore, Torii et al.[23] employed frame model to optimize a skeletal structure under global stability constraint in which the Euler formula is not needed. Madah et al.[24] simulated each truss member by the geometrically nonlinear beam element and obtained the optimal solution in a similar way. Note that the aforementioned works can be regarded as deterministic optimization which does not consider uncertainty in structural properties or loading conditions. However, it is more reasonable to incorporate uncertainty during structural optimization process since it is unavoidable in the real world structure.

Recently, a large number of studies have been carried out for design and optimization of structures taking uncertainty into account.[25-27] The optimization methods considering uncertainty can be generally divided into two categories according to the models for characterizing the uncertainty. When the probabilistic model is used, the uncertainty is assumed to obey some predefined distribution, and the objective and constraint functions are usually formulated as the functions of statistical moments or probability of failure of the structural response, which are regarded as robust design optimization (RDO)[28] or reliability-based design optimization (RBDO).[29,30] In addition, some researchers also utilize stochastic methods to explicitly propagate the structural uncertainty to structural response.[31,32] Since the exact distribution information of uncertainty may be unknown in advance, a large estimation error would occur in both RDO and RBDO when the assumed distribution of uncertainty is far away from the real one.[33] On the other hand, the worst case optimization (WCO) provides an alternative if the uncertainty is described by a non-probabilistic model, which aims at minimizing the maximum (worst) objective value among all the possible realizations of uncertainty which would result in a structure less sensitive to the uncertainty[34]; hence, WCO can be also categorized into RDO. In order to save computational efforts in searching the worst value, Kanno and Takewaki[35,36] constructed a minimum confidence ellipsoid of the structural response to solve the WCO problem in a confidence way, and the uncertainty is considered in the cross-sectional areas and the applied load; Guo et al.[37] extended this method to a single-level problem formulation with stiffness uncertainty and fixed nodes configuration; Kanno and Guo[38] reduced the discrete WCO of truss structure to a mix-integer problem where the uncertain load is predefined in an ellipsoid. Although these WCO with confidence robustness model can be successfully solved, incorporating with geometry optimization and the nodal uncertainty, which is another common source of uncertainty, should also be considered. Fu et al.[39] solved the truss topology optimization problem with uncertain nodal locations using proportional topology optimization method, where the inverse of stiffness matrix is expressed based on Neumann series expansion. However, since the objective is the expected value of structural response, this method might be insufficient to characterize the uncertain properties of the structure if the deviation of response is moderately large. Recently Yamakawa and Ohsaki[40-42] developed an order statistic approach to consider the worst case value with certain confidence level, in which the worst value is approximated by the kth order statistics and the parameter k is regarded as the robustness level according to the theory of distribution-free tolerance interval. This method can be regarded as a special case of scenario optimization where the scenario theory is used to provide a certain robustness for the optimal solution, that is the probability of the solution not to violate the requirements in the unseen future, with given sample set and confidence level.[43] However, the uncertainty is only assumed in the objective function in order to limit the difficulty.

In the present study, we propose a worst case method for robust geometry and topology optimization of plane frames to minimize the maximum stress under volume and global stability constraints, where the uncertainty is assumed to exist in nodal locations and cross-sectional areas. The order statistics corresponding to the specific robustness level are used for the objective function and the global stability constraint. Geometry of the frame structure is determined by the FDM which is applied to the auxiliary truss structure that is irrelevant to the true loading and boundary conditions of the frame

structure to be optimized; thus the design variables are the force densities of the members of the auxiliary pin-jointed structure and the cross-sectional areas of the frame. The performance and properties of robust geometry and topology are investigated in comparison to those without considering uncertainty. Note that in this paper we solve the RDO problem using a randomized approach. We do not make any prior assumption on the distribution information of uncertainties in nodal locations and cross-sectional areas, but only assume that they are independent and identically distributed (i.i.d) to provide randomization in the structural response.

The rest of the paper is organized as follows. In Section 2 the basic idea of FDM is briefly introduced. The formulation of robust optimization problem, as well as the definitions of stiffness uncertainty and the relaxed approximation of worst value using order statistics, are given in Section 3. In Section 4, two numerical alternatives to handle stress and global instability phenomena are given and illustrated, and three numerical examples are explored in Section 5 to verify the effectiveness of the proposed method. Finally, some conclusions are drawn in Section 6.

2 | FDM FOR AUXILIARY TRUSS STRUCTURE

FDM is originally used in the form-finding process of cable nets and tensegrity structures, in which the force density is defined as the axial force divided by the member length. Because axial force, shear force, and bending moment exist in the frame structure, in this study the FDM is applied to an auxiliary pin-jointed structure to define the nodal locations of the frame that is to be optimized. Therefore, it is worth noting again that the structure considered in this section is a pin-jointed truss structure.

Let m and n represent the numbers of members and nodes of the auxiliary pin-jointed truss structure, respectively. If member i connects nodes j and k, then the m-by-n connectivity matrix $\boldsymbol{C}$ is given by defining each entry as[11,13,44]

$$\boldsymbol{C}_{(i,p)} = \begin{cases} 1 & p = j \\ -1 & p = k \\ 0 & \text{other case} \end{cases} \quad (i = 1, 2, \ldots, m; j, k = 1, 2, \ldots, n) \tag{1}$$

where the subscript (i, p) indicates the entry of $\boldsymbol{C}$ at the ith row and pth column. The force density q_i of the ith member is defined as

$$q_i = \frac{N_i}{L_i} \tag{2}$$

where N_i is the axial force and L_i is the length of the ith member. Accordingly, the m-by-1 force density vector is denoted by $\boldsymbol{q} = (q_1, q_2, \ldots, q_m)^T$. Let $\boldsymbol{x}_{\text{free}}, \boldsymbol{x}_{\text{fix}}, \boldsymbol{y}_{\text{free}}$, and $\boldsymbol{y}_{\text{fix}}$ represent the x- and y-coordinates of the free nodes and the fixed nodes, respectively, and arrange the columns of connectivity matrix $\boldsymbol{C}$ such that the columns corresponding to the free nodes precede those corresponding to the fixed nodes, that is, $\boldsymbol{C} = (\boldsymbol{C}_{\text{free}}, \boldsymbol{C}_{\text{fix}})$. Then the equilibrium equations at the free nodes and the fixed nodes of the auxiliary pin-jointed truss structure are written as[11,44]

$$\begin{aligned} \boldsymbol{C}_{\text{free}}^T \text{diag}(\boldsymbol{q}) \boldsymbol{C}_{\text{free}} \boldsymbol{x}_{\text{free}} + \boldsymbol{C}_{\text{free}}^T \text{diag}(\boldsymbol{q}) \boldsymbol{C}_{\text{fix}} \boldsymbol{x}_{\text{fix}} &= \boldsymbol{P}_{x,\text{free}} \\ \boldsymbol{C}_{\text{free}}^T \text{diag}(\boldsymbol{q}) \boldsymbol{C}_{\text{free}} \boldsymbol{y}_{\text{free}} + \boldsymbol{C}_{\text{free}}^T \text{diag}(\boldsymbol{q}) \boldsymbol{C}_{\text{fix}} \boldsymbol{y}_{\text{fix}} &= \boldsymbol{P}_{y,\text{free}} \\ \boldsymbol{C}_{\text{fix}}^T \text{diag}(\boldsymbol{q}) \boldsymbol{C}_{\text{free}} \boldsymbol{x}_{\text{free}} + \boldsymbol{C}_{\text{fix}}^T \text{diag}(\boldsymbol{q}) \boldsymbol{C}_{\text{fix}} \boldsymbol{x}_{\text{fix}} &= \boldsymbol{P}_{x,\text{fix}} \\ \boldsymbol{C}_{\text{fix}}^T \text{diag}(\boldsymbol{q}) \boldsymbol{C}_{\text{free}} \boldsymbol{y}_{\text{free}} + \boldsymbol{C}_{\text{fix}}^T \text{diag}(\boldsymbol{q}) \boldsymbol{C}_{\text{fix}} \boldsymbol{y}_{\text{fix}} &= \boldsymbol{P}_{y,\text{fix}} \end{aligned} \tag{3}$$

where $\text{diag}(\boldsymbol{q})$ is the square diagonal matrix with the elements of vector $\boldsymbol{q}$ on the main diagonal, and $\boldsymbol{P}_{x,\text{free}}$, $\boldsymbol{P}_{x,\text{fix}}$, $\boldsymbol{P}_{y,\text{free}}$, and $\boldsymbol{P}_{y,\text{fix}}$ are the external forces applied at the free nodes and fixed nodes in x- and y-directions, respectively. See References 11, 44 for details and illustrative examples for Equation (3). Unlike the traditional FDM, the fixed nodes here consist of the support nodes and loaded nodes, and therefore $\boldsymbol{P}_{x,\text{free}}$ and $\boldsymbol{P}_{y,\text{free}}$ are zero vectors. If the force densities are given for all members in the structure and the locations of fixed nodes are assigned, then the locations of free nodes can be obtained from Equation (3), that is

$$\begin{aligned} \boldsymbol{x}_{\text{free}} &= -(\boldsymbol{C}_{\text{free}}^T \text{diag}(\boldsymbol{q}) \boldsymbol{C}_{\text{free}})^{-1} \boldsymbol{C}_{\text{free}}^T \text{diag}(\boldsymbol{q}) \boldsymbol{C}_{\text{fix}} \boldsymbol{x}_{\text{fix}} \\ \boldsymbol{y}_{\text{free}} &= -(\boldsymbol{C}_{\text{free}}^T \text{diag}(\boldsymbol{q}) \boldsymbol{C}_{\text{free}})^{-1} \boldsymbol{C}_{\text{free}}^T \text{diag}(\boldsymbol{q}) \boldsymbol{C}_{\text{fix}} \boldsymbol{y}_{\text{fix}} \end{aligned} \tag{4}$$

It has been proved in Reference 45 that the matrix $\boldsymbol{C}_{\text{free}}^{T}\text{diag}(\boldsymbol{q})\boldsymbol{C}_{\text{free}}$ is nonsingular if at least one node is fixed and $\boldsymbol{q}$ is a non-zero vector, resulting in the existence of a solution for $\boldsymbol{x}_{\text{free}}$ and $\boldsymbol{y}_{\text{free}}$ in Equation (4). Also, it is pointed out in Reference 13 that if the axial force N_i in Equation (3) is non-zero and the upper and lower bounds for q_i have the same absolute value, then a lower bound for the member length L_i can be indirectly assigned to prevent generating extremely short members.

3 | ROBUST GEOMETRY AND TOPOLOGY OPTIMIZATION OF PLANE FRAME

One of the formulations for robust optimization is to minimize structural cost under constraint on worst value of structural response, which is also called WCO or worst case design. Accordingly, we present an optimization problem of minimizing the maximum stress of plane frame under volume and global stability constraints, and the worst values are used for evaluations of the objective function and the linear buckling load factor. The cross-section is assumed to be circular solid and the second moment of inertia can be expressed in terms of the cross-sectional area.

3.1 | Uncertainty in member stiffness

In this study, the uncertainty is considered in the nodal locations and the cross-sectional areas. Details of modeling uncertainty are illustrated below.

Figure 1(A) illustrates the ith frame member in the global coordinates (x,y), connecting nodes $i1$ and $i2$ and has the length L_i. We first add randomness to the x- and y-coordinates of the end nodes $i1$ and $i2$ and express the uncertain locations of these nodes as

$$(x_j', y_j') = (x_j, y_j) + (\Delta x_j, \Delta y_j) \quad \text{for} \quad j = i1, i2 \tag{5}$$

where (x_j', y_j') is the uncertain location of node j and (x_j, y_j) is the corresponding value without uncertainty, and they are indicated by the blue and red dots in Figure 1(A), respectively; $(\Delta x_j, \Delta y_j)$ represents the random variable of uncertainty in nodal locations.

The ith member with length L_i' is evenly divided into four Euler-Bernoulli beam elements by the intermediate nodes $i3$, $i4$, and $i5$, as shown by the red dots in Figure 1(B), and their locations are obtained by the interpolation between (x_{i1}', y_{i1}') and (x_{i2}', y_{i2}') as follows:

$$(x_j', y_j') = (x_{i1}', y_{i1}') + k\left[\frac{(x_{i1}', y_{i2}') - (x_{i1}', y_{i1}')}{4}\right], k = 1, 2, 3 \tag{6}$$

where (x_{i1}', y_{i1}') and (x_{i2}', y_{i2}') are the uncertain locations of end nodes $i1$ and $i2$ obtained from Equation (5), and $k = 1$, 2, and 3 correspond to the locations of $i3$, $i4$, and $i5$, respectively. Given the upper-bound eccentricity e, the uncertain locations of intermediate nodes $i3$, $i4$, and $i5$ are also defined by respectively adding randomness to their x- and y-coordinates perpendicular to the ith member within the range of $e \times L_i'$ as

$$\begin{gathered}(x_j'', y_j'') = (x_j', y_j') + (\Delta x_j, \Delta y_j) \text{ for } j = i3, i4, i5 \\ \sqrt{\Delta x_j{}^2 + \Delta y_j{}^2} \le e \times L_i'; \quad (\Delta x_j, \Delta y_j) \perp (x_{i2}' - x_{i1}', y_{i2}' - y_{i1}')\end{gathered} \tag{7}$$

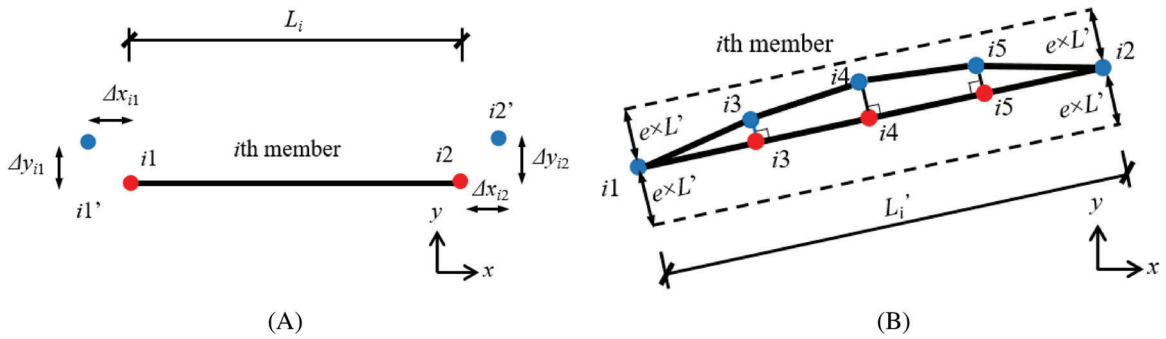

FIGURE 1 Uncertainty in nodal locations of the ith member on (A) end nodes; (B) intermediate nodes

where (x_j'', y_j'') $(j = i3, i4, i5)$ are the uncertain locations of nodes $i3$, $i4$, and $i5$ indicated by the blue dots in Figure 1(B). Accordingly, the uncertainties in the locations of nodes $i3$, $i4$, and $i5$ consist of two parts: one is the uncertainty in locations of nodes $i1$ and $i2$, and the other is the randomness directly imposed on the nodes as shown in Figure 1(B).

Finally, the imperfect geometry of the ith member is obtained through the uncertain locations of nodes $i1$ to $i5$ in Figure 1(B). Besides, correlation among uncertainties in both end nodes and intermediate nodes should be appropriately considered. Since we use a randomization approach for finding the worst values of responses, the correlation coefficient is described by the following exponential decay function.[46]

$$c_{j1j2} = \exp\left(-\frac{\|(x_{j1}, y_{j1}) - (x_{j2}, y_{j2})\|}{L_{\text{exp}}}\right), \quad j1, j2 = i1, i2, \ldots, i5 \tag{8}$$

where c_{j1j2} is the correlation coefficient of uncertainty between nodes $j1$ and $j2$, and L_{exp} is the correlation length. Clearly, a larger L_{exp} indicates a stronger correlation, and because the correlation among uncertainties in skeletal structures is relatively weaker than in continua,[46] a small value is used in the numerical examples.

As for uncertainty in cross-sectional area of the ith member, the randomness is added in a similar manner as Equation (5), that is

$$A_i' = A_i + \Delta A_i \tag{9}$$

where A_i' is the uncertain cross-sectional area of the ith member and A_i is the corresponding value without uncertainty; ΔA_i is the random variable that represents uncertainty in cross-sectional area. Note that the four elements of the ith member in Figure 1(B) share the same uncertain cross-sectional area A_i'.

The procedure for incorporating uncertainty in nodal locations and cross-sectional area of the ith member is summarized as follows:

(i) Calculate the length of the ith frame member L_i, and determine the uncertain locations of the end nodes $i1$ and $i2$ by using Equations (5) and (8).
(ii) Calculate the length of the ith frame member L_i' after completing step (i), and evenly divide it into four beam elements and obtain the locations of intermediate nodes $i3$ to $i5$ using Equation (6). Calculate the corresponding uncertain locations of nodes $i3$ to $i5$ by using Equations (7) and (8).
(iii) Determine the uncertain cross-sectional area of the ith frame member by using Equation (9), and assign it to the four beam elements.

In the numerical examples, uniform distributions are assumed for the uncertain parameters in the feasible domain.

3.2 | Problem formulation

We begin with the deterministic geometry and topology optimization problem of minimizing the stress of a plane frame under global stability and volume constraints, which is formulated as follows:

$$\begin{aligned}
&\text{Minimize } \sigma = \max_{\substack{i=1,2,\cdots m_e \\ j=1,2,\cdots p}} (\sigma_{V,ij}(\boldsymbol{x}_{\text{free}}, \boldsymbol{y}_{\text{free}}, \boldsymbol{A})) \\
&\text{subject to } \frac{1}{\lambda^{\text{cr}}(\boldsymbol{x}_{\text{free}}, \boldsymbol{y}_{\text{free}}, \boldsymbol{A})} \le \frac{1}{\lambda_{\text{L}}}; \quad V(\boldsymbol{x}_{\text{free}}, \boldsymbol{y}_{\text{free}}, \boldsymbol{A}) \le V_{\text{U}}; \\
&\qquad \underline{\boldsymbol{x}}_{\text{free}} \le \boldsymbol{x}_{\text{free}} \le \overline{\boldsymbol{x}}_{\text{free}}; \quad \underline{\boldsymbol{y}}_{\text{free}} \le \boldsymbol{y}_{\text{free}} \le \overline{\boldsymbol{y}}_{\text{free}}; \quad \underline{\boldsymbol{A}} \le \boldsymbol{A} \le \overline{\boldsymbol{A}}
\end{aligned} \tag{10}$$

where $\boldsymbol{x}_{\text{free}}$, $\boldsymbol{y}_{\text{free}}$, and $\boldsymbol{A}$ are the vectors of x- and y-coordinates of the free nodes and the cross-sectional areas of the Euler-Bernoulli beam elements, respectively, and the lower and upper bars in the constraints represent the corresponding lower and upper bounds of the design variables; m_e is the number of beam elements in the frame; p is the number of points for stress evaluation within each element and their selection will be explained in Section 4; $\sigma_{V,ij}$ is the von Mises stress evaluated at point j of the ith element, and the detailed implementation of calculating the von Mises stress of beam

element is referred to Reference 47; V_U and λ_L are the upper bound for the structural volume and the lower bound for the global linear buckling load factor λ^{cr}, respectively. Note that λ^{cr} is defined as the smallest positive eigenvalue of the following eigenvalues problem:

$$(\boldsymbol{K}(\boldsymbol{x}_{free}, \boldsymbol{y}_{free}, \boldsymbol{A}) + \lambda \boldsymbol{K}_G(\boldsymbol{x}_{free}, \boldsymbol{y}_{free}, \boldsymbol{A}))\boldsymbol{\Phi} = \boldsymbol{0} \tag{11}$$

where $\boldsymbol{K}$ and $\boldsymbol{K}_G$ are the elastic stiffness matrix and the geometrical stiffness matrix corresponding to the unit load factor, respectively.[48] In Equation (10), the global stability constraint is written with respect to the reciprocals of λ^{cr} and λ_L to ensure that λ^{cr} is either larger than λ_L or negative,[19] and for simplicity we hereafter denote the reciprocals as $\gamma^{cr} = 1/\lambda^{cr}$ and $\gamma_U = 1/\lambda_L$, respectively.

By incorporating the FDM in Section 2, the locations of free nodes of a plane frame can be derived by solving Equation (4) of the corresponding auxiliary truss, and the optimization problem (10) is restated as

$$\begin{aligned}
&\text{Minimize } \sigma = \max_{\substack{i=1,2,\cdots m_e \\ j=1,2,\cdots p}} (\sigma_{V,ij}(\boldsymbol{x}_{free}(\boldsymbol{q}), \boldsymbol{y}_{free}(\boldsymbol{q}), \boldsymbol{A})) \\
&\text{subject to } \gamma^{cr}(\boldsymbol{x}_{free}(\boldsymbol{q}), \boldsymbol{y}_{free}(\boldsymbol{q}), \boldsymbol{A}) \le \gamma_U; \quad V(\boldsymbol{x}_{free}(\boldsymbol{q}), \boldsymbol{y}_{free}(\boldsymbol{q}), \boldsymbol{A}) \le V_U \\
&\qquad \underline{\boldsymbol{q}} \le \boldsymbol{q} \le \overline{\boldsymbol{q}}; \quad \underline{\boldsymbol{A}} \le \boldsymbol{A} \le \overline{\boldsymbol{A}}
\end{aligned} \tag{12}$$

where $\boldsymbol{q}$ is the force density vector. As stated in Reference 13, problems (10) and (12) are basically the same and will lead to the same solution if a set of $\boldsymbol{q}$ in problem (12) can define the optimal solution of problem (10), which means the optimal solution of problem (10) can be found by solving problem (12) if it is included in the feasible domain of problem (12). Note again that in problem (12) the stresses are calculated for the rigidly jointed frame model with Euler-Bernoulli beam elements.

When uncertainty, which is illustrated in Section 3.1, is introduced to problem (12), the optimization problem considering uncertainty takes the following form:

$$\begin{aligned}
&\text{Minimize } \sigma^{max} = \max_{\theta \in \Omega} \sigma(\boldsymbol{x}_{free}(\boldsymbol{q}), \boldsymbol{y}_{free}(\boldsymbol{q}), \boldsymbol{A}; \boldsymbol{\theta}) \\
&\text{subject to } \gamma^{cr,max} = \max_{\theta \in \Omega} (\gamma^{cr}(\boldsymbol{x}_{free}(\boldsymbol{q}), \boldsymbol{y}_{free}(\boldsymbol{q}), \boldsymbol{A}; \boldsymbol{\theta})) \le \gamma_U; \\
&\qquad V(\boldsymbol{x}_{free}(\boldsymbol{q}), \boldsymbol{y}_{free}(\boldsymbol{q}), \boldsymbol{A}) \le V_U; \ \underline{\boldsymbol{q}} \le \boldsymbol{q} \le \overline{\boldsymbol{q}}; \ \underline{\boldsymbol{A}} \le \boldsymbol{A} \le \overline{\boldsymbol{A}}
\end{aligned} \tag{13}$$

where σ and γ^{cr} are the same as problem (12); $\boldsymbol{\theta} = (\Delta\boldsymbol{x}, \Delta\boldsymbol{y}, \Delta\boldsymbol{A})$ is the vector representing the uncertainty in nodal locations and cross-sectional areas; Ω is the corresponding uncertain parameter space of $\boldsymbol{\theta}$; σ^{max} and $\gamma^{cr,max}$ are the values of maximum von Mises stress and reciprocal of global linear load factor within the space Ω, respectively. It is worth noting that problem (13) can be regarded as a WCO problem with semi-infinite constraint for design variables and uncertain parameters, since it can be equivalently transformed into

$$\begin{aligned}
&\text{Minimize } \sigma^{max} = \max_{\theta \in \Omega} \sigma(\boldsymbol{x}_{free}(\boldsymbol{q}), \boldsymbol{y}_{free}(\boldsymbol{q}), \boldsymbol{A}; \boldsymbol{\theta}) \\
&\text{subject to } \gamma^{cr} = (\gamma^{cr}(\boldsymbol{x}_{free}(\boldsymbol{q}), \boldsymbol{y}_{free}(\boldsymbol{q}), \boldsymbol{A}; \boldsymbol{\theta})) \le \gamma_U \text{ for } \forall \boldsymbol{\theta} \in \Omega; \\
&\qquad V(\boldsymbol{x}_{free}(\boldsymbol{q}), \boldsymbol{y}_{free}(\boldsymbol{q}), \boldsymbol{A}) \le V_U; \underline{\boldsymbol{q}} \le \boldsymbol{q} \le \overline{\boldsymbol{q}}; \ \underline{\boldsymbol{A}} \le \boldsymbol{A} \le \overline{\boldsymbol{A}}
\end{aligned} \tag{14}$$

By introducing the slack variable t, problem (14) can be further reformulated as follows, where the constraints are to be satisfied for all possible set of uncertain parameters:

$$\begin{aligned}
&\text{Minimize } t \\
&\text{subject to } \sigma(\boldsymbol{x}_{free}(\boldsymbol{q}), \boldsymbol{y}_{free}(\boldsymbol{q}), \boldsymbol{A}; \boldsymbol{\theta}) \le t \text{ for } \forall \boldsymbol{\theta} \in \Omega; \\
&\qquad \gamma^{cr} = (\gamma^{cr}(\boldsymbol{x}_{free}(\boldsymbol{q}), \boldsymbol{y}_{free}(\boldsymbol{q}), \boldsymbol{A}; \boldsymbol{\theta})) \le \gamma_U \text{ for } \forall \boldsymbol{\theta} \in \Omega; \\
&\qquad V(\boldsymbol{x}_{free}(\boldsymbol{q}), \boldsymbol{y}_{free}(\boldsymbol{q}), \boldsymbol{A}) \le V_U; \underline{\boldsymbol{q}} \le \boldsymbol{q} \le \overline{\boldsymbol{q}}; \ \underline{\boldsymbol{A}} \le \boldsymbol{A} \le \overline{\boldsymbol{A}}
\end{aligned} \tag{15}$$

which is classified as an RDO problem. Therefore, we solve an RDO problem using the randomized or stochastic approach for estimating the worst values of the responses of the WCO problem. However, it is difficult to directly solve problem (15) because the exact worst values of structural responses are difficult to find. Therefore, in this study the exact worst

responses are relaxed to the 100βth percentile structural responses which are approximated by order statistics, and it will be illustrated in the next section.

3.3 | Worst value approximation using order statistics

We use a randomization approach for finding the worst values of responses. Let $\boldsymbol{\theta}_1, \boldsymbol{\theta}_2, \ldots, \boldsymbol{\theta}_{m_s}$ be the m_s samples of independent and identically distributed (i.i.d.) vectors of uncertainty in nodal locations and cross-sectional areas with unknown distributions, and $(\boldsymbol{q}, \boldsymbol{A})$ be the design variable vectors of force densities and cross-sectional areas. The corresponding m_s structural responses in Equation (15) with respect to $\boldsymbol{\theta}_1, \boldsymbol{\theta}_2, \ldots, \boldsymbol{\theta}_{m_s}$ and $(\boldsymbol{q}, \boldsymbol{A})$ are denoted by $\sigma_1 = \sigma(\boldsymbol{q}, \boldsymbol{A}; \boldsymbol{\theta}_1), \ldots, \sigma_{m_s} = \sigma(\boldsymbol{q}, \boldsymbol{A}; \boldsymbol{\theta}_{m_s})$ and $\gamma_1^{\mathrm{cr}} = \gamma^{\mathrm{cr}}(\boldsymbol{q}, \boldsymbol{A}; \boldsymbol{\theta}_1), \ldots, \gamma_{m_s}^{\mathrm{cr}} = \gamma^{\mathrm{cr}}(\boldsymbol{q}, \boldsymbol{A}; \boldsymbol{\theta}_{m_s})$, respectively. Furthermore, we define $\sigma_{1:m_s}, \sigma_{2:m_s}, \ldots, \sigma_{m_s:m_s}$ as a permutation of $\sigma_1, \sigma_2, \ldots, \sigma_{m_s}$ in a descending order, that is, $\sigma_{1:m_s} \geq \sigma_{2:m_s} \geq \ldots \geq \sigma_{m_s:m_s}$, and the kth maximum stress $\sigma_{k:m_s}$ is called the kth order statistic of the stress. The $\gamma_{1:m_s}^{\mathrm{cr}}, \gamma_{2:m_s}^{\mathrm{cr}}, \ldots, \gamma_{m_s:m_s}^{\mathrm{cr}}$ and $\gamma_{k:m_s}^{\mathrm{cr}}$ are also defined in the same manner. Note that the descending order statistics are used herein for convenience to approximate the worst values of the stress and the linear buckling load factor, which is different from the conventional definition of order statistics that is arranged in an ascending order.

Since $\sigma_{1:m_s}, \sigma_{2:m_s}, \ldots, \sigma_{m_s:m_s}$ are derived from the same function with different vectors of uncertain parameter, it is reasonable to assume that $\sigma_{1:m_s}, \sigma_{2:m_s}, \ldots, \sigma_{m_s:m_s}$ are m_s realizations of the random variable Y_σ because the function of random variables is still a random variable, and the unknown cumulative distribution function (CDF) of Y_σ is denoted by $F_\sigma(y_\sigma) = \Pr\{Y_\sigma \leq y_\sigma\}$. According to the statistical inference theory in order statistics,[49] the probability α_k of $100\beta\%$ of the structural stress σ less than the kth order statistic of structural stress $\sigma_{k:m_s}$ can be calculated as

$$\Pr\{F_\sigma(\sigma_{k:m_s}) \geq \beta\} = \sum_{r=0}^{m_s-k} \binom{m_s}{r} \beta^r (1-\beta)^{m_s-r} = 1 - I_\beta(m_s - k + 1, k) = \alpha_k \tag{16}$$

where $I_\beta(m_s - k + 1, k)$ is the incomplete beta function.[41,49] Similarly, we assume that $\gamma_{1:m_s}^{\mathrm{cr}}, \gamma_{2:m_s}^{\mathrm{cr}}, \ldots, \gamma_{m_s:m_s}^{\mathrm{cr}}$ are m_s realizations of the random variables Y_γ with unknown CDF $F_\gamma(y_\gamma) = \Pr\{Y_\gamma \leq y_\gamma\}$, and the probability α_k of $100\beta\%$ of γ^{cr} less than the kth order statistics $\gamma_{k:m_s}^{\mathrm{cr}}$ can be calculated as

$$\Pr\{F_\gamma(\gamma_{k:m_s}^{\mathrm{cr}}) \geq \beta\} = \sum_{r=0}^{m_s-k} \binom{m_s}{r} \beta^r (1-\beta)^{m_s-r} = 1 - I_\beta(m_s - k + 1, k) = \alpha_k \tag{17}$$

Equations (16) and (17) are also called distribution-free one-side tolerance interval because the probability of the structural response falling into the one-side interval $(-\infty, \sigma_{k:m_s})$ or $(-\infty, \gamma_{k:m_s}^{\mathrm{cr}})$ is free of the definition of F_σ or F_γ, respectively, and the kth order statistics $\sigma_{k:m_s}$ and $\gamma_{k:m_s}^{\mathrm{cr}}$ can be seen as the 100βth percentile structural response in probabilistic sense and α_k is regarded as the confidence level. In order words, if the structural responses are randomly generated corresponding to unknown m_s vectors of uncertain parameters $\boldsymbol{\theta}_1, \boldsymbol{\theta}_2, \ldots, \boldsymbol{\theta}_{m_s}$, one can estimated the 100βth percentile of the structural response with confidence level α_k by Equations (16) and (17) using order statistics where randomness is considered in both $\boldsymbol{\theta}_1, \boldsymbol{\theta}_2, \ldots, \boldsymbol{\theta}_{m_s}$ and structural response. Obviously, if α_k and β are large enough, for example, 0.9 or 0.95, the kth order statistics can provide an accurate quantile response as relaxation of worst values in problems (13) and (15).

Moreover, as demonstrated by Ohsaki et al.,[40,41] β is a decreasing function of k with given sample size m_s and confidence level α_k, which indicates that a higher order k corresponds to a less 100βth percentile structural response under uncertainty. Therefore, the order k and its corresponding order statistic approximating the 100βth percentile of structural response can be regarded as representing the robustness level of the structure. Suppose the worst values of the responses in the parameter space in problem (15) are approximated by the kth order statistics $\sigma_{k:m_s}$ and $\gamma_{k:m_s}^{\mathrm{cr}}$ among m_s realizations at confidence level α_k. Then problem (15) can be rewritten as

$$\begin{aligned}
&\text{Minimize } t \\
&\text{subject to } \sigma_{k:m_s}(\boldsymbol{x}_{\mathrm{free}}(\boldsymbol{q}), \boldsymbol{y}_{\mathrm{free}}(\boldsymbol{q}), \boldsymbol{A}; \boldsymbol{\Theta}) \leq t; \\
&\qquad \gamma_{k:m_s}^{\mathrm{cr}}(\boldsymbol{x}_{\mathrm{free}}(\boldsymbol{q}), \boldsymbol{y}_{\mathrm{free}}(\boldsymbol{q}), \boldsymbol{A}; \boldsymbol{\Theta}) \leq \gamma_{\mathrm{U}}; \\
&\qquad V(\boldsymbol{x}_{\mathrm{free}}(\boldsymbol{q}), \boldsymbol{y}_{\mathrm{free}}(\boldsymbol{q}), \boldsymbol{A}) \leq V_{\mathrm{U}}; \underline{\boldsymbol{q}} \leq \boldsymbol{q} \leq \overline{\boldsymbol{q}};\ \ \underline{\boldsymbol{A}} \leq \boldsymbol{A} \leq \overline{\boldsymbol{A}}
\end{aligned} \tag{18}$$

where $\boldsymbol{\Theta} = (\boldsymbol{\theta}_1, \cdots, \boldsymbol{\theta}_{m_s})$ denotes the set of m_s sample vectors of uncertain parameters. The difference between the approximated worst values in problem (18) and the exact worst values in problem (15) will become smaller if the value of k is closer to 1, and the robustness levels of both maximum stress and global stability also increase as the order k decreases. Note that the constraints in RDO problem (15) are relaxed, that is, the robustness for satisfying the constraints is relaxed, by using order statistics in problem (18) at specified confidence level α_k and such robustness can be referred to as statistical feasibility robustness which handles the semi-infinite constraints stochastically.[50] Although similar formulation to incorporate uncertainty in constraint can be found in RBDO problem and referred to as risk or chance constraint,[51-53] there is no general consensus that RBDO should not be considered as part of the robust optimization methodology, and vice versa,[50] and the connection between robustness and the stochastic or probability theory are also exploited recently by some researchers.[54] The equivalence between the probabilistic optimization problem and the robust optimization with uncertain-but-bounded variables are also discussed by Elishakoff and Ohsaki.[27] Hence, in this study we consider problem (18) as robust optimization problem due to the fact that it is a relaxed version of the WCO problem (15), and problem (18) serves as the RDO problem to be solved in the rest of the paper.

As pointed out in Reference 13, closely spaced nodes may exist when the value of N_i in Equation (2) is very small, although the member length is indirectly controlled by the bounds of force densities to prevent the existence of zero-length member. Moreover, if the cross-sectional area of the short member is moderately large, unexpectedly large von Mises stress may appear due to its large bending stiffness. However, the closely spaced nodes in the final solution will be merged into one node to obtain a simplified structural layout without short members. Therefore, in order to find the appropriate maximum stress to be minimized, the stress of the short member is set to 0 and then ignored in this study during the optimization process. In addition, unlike the frame member in Section 3.1 which is divided into four beam elements, the short member is modeled by only one beam element to avoid singularity caused by its large stiffness, and the nodal uncertainty is then applied only at the end nodes of a short member.

4 | PENALIZATION OF STRESS AND GEOMETRICAL STIFFNESS

In the preceding section we formulated an RDO problem by combing the FDM and order statistics to approximate the quantile responses as a relaxed worst values of the structural responses. Since singularity phenomena might emerge in the maximum stress and the global buckling load factor and influence the optimization result, the existing approach for stress singularity problem is incorporated and extended to alleviate singularity in global buckling factor.

4.1 | Penalization of stress

The stress singularity phenomenon has been extensively studied for both continuum and skeletal structures.[20,55] Based on the method for stress-based optimization in Reference 55, the element stress is penalized as follows if the cross-sectional area of the ith element is small enough:

$$\widehat{\sigma}_{V,i} = (A_i/\overline{A}_i)^{\eta} \max_{j=1,2,\cdots p} (\sigma_{V,ij}) \tag{19}$$

where i, j, p and $\sigma_{V,ij}$ have the same meaning as Equations (10) and (12); $\overline{A}_i$ is the ith element of $\overline{\boldsymbol{A}}$ defined in Equation (18); η is the penalization parameter to underestimate the stress of a thin element. According to Reference 55, the value of η should be greater than 0 and less than 1, and in this study we select $\eta = 0.5$ which is the same as in Reference 55.

To verify the effectiveness of using Equation (19), a simple example of stress minimization problem under volume constraint is to be solved where uncertainty is not taken into consideration. The initial structure of a simple frame is shown in Figure 2(A), in which the node number and the member number are indicated by those with and without parentheses, respectively. The frame is pin-supported at nodes 1 and 2, and a downward vertical load F with magnitude 2000 N is applied at node 3. The design variables are the cross-sectional areas of the five members, and each member is divided into four Euler-Bernoulli beam elements. Note that the crossing members 3 and 4 are not connected at their intersection. As a result, there are 20 beam elements in total in the structure. The Young's modulus is 3×10^{11} Pa, and the von Mises stress is calculated at the neutral axis and the upper and lower edges of the cross-section at the two end nodes of each element, which are illustrated in Figure 2(B). The optimization problem is formulated based on Equation (12) in Section 3.2 without global buckling constraint and considering only $\boldsymbol{A}$ as design variables, where $m_e = 20$, $p = 6$, and the

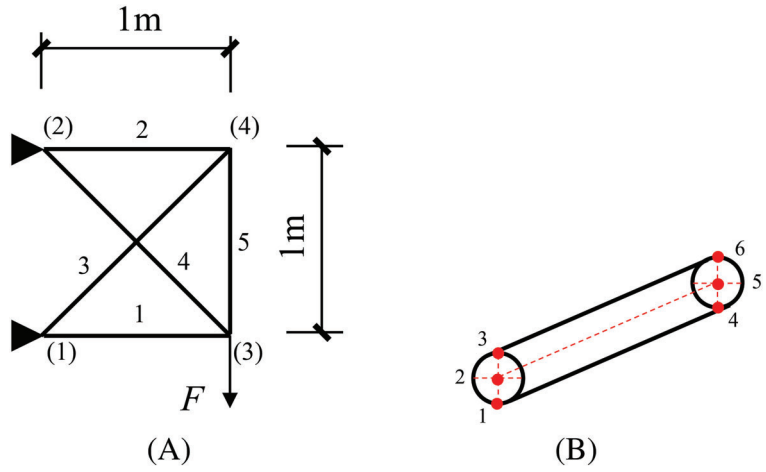

FIGURE 2 A simple frame model: (A) initial structure; (B) stress evaluation points of each element

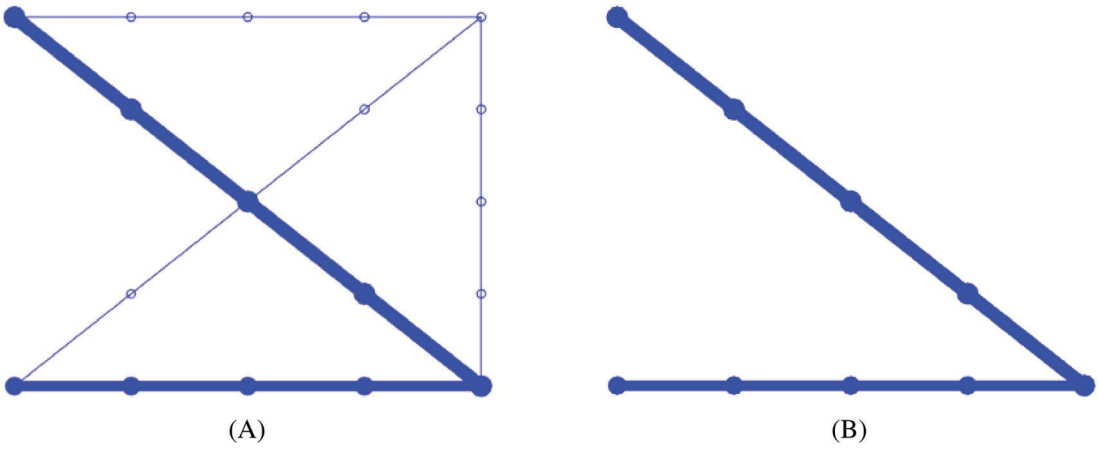

FIGURE 3 Optimal solution of simple frame example: (A) before removing thin elements; (B) after removing thin elements

TABLE 1 Cross-sectional areas of optimal solution of simple frame example

Member number	Cross-sectional area (m^2)
1	0.03478
2	1×10^{-7}
3	1×10^{-7}
4	0.04611
5	1×10^{-7}

upper and lower bounds of cross-sectional areas for all members are 0.05 m^2 and 1×10^{-7} m^2, respectively. The stress of a thin element is penalized using Equation (19), and the thin elements are defined as those whose cross-sectional areas are less than 1% of A_{max}, where A_{max} is the maximum cross-sectional area of the frame. The problem is solved by the generalized reduced gradient (GRG) method of CONOPT in the MATLAB interface of TOMLAB with default settings.[56]

The optimal solution and the corresponding cross-sectional areas are shown in Figure 3(A) and Table 1, and the result after removing the thin elements is shown in Figure 3(B). The maximum von Mises stresses before and after removing thin elements are 68,199.41 Pa and 68,199.54 Pa, respectively, which are almost the same, indicating that the stress singularity phenomenon can be avoided by using Equation (19).

4.2 | Penalized geometrical stiffness

The penalization approach to alleviate stress singularity is extended here for singularity phenomenon in global instability. It has been pointed out that the emergence of slender member in compression will lead to a violation of global stability

constraint due to their negative contribution in stiffness matrix.[17] Therefore, in order to obtain the accurate linear buckling load factor of the structure when thin elements are involved, the geometrical stiffness of the thin element, say the ith element, is penalized as follows:

$$\widehat{\boldsymbol{K}}_{G,i} = (A_i/\overline{A}_i)^{\rho} \times \boldsymbol{K}_{G,i} \tag{20}$$

where $\boldsymbol{K}_{G,i}$ is the original geometrical stiffness matrix of the ith element and ρ is the penalization parameter. Equation (20) is inspired by the standard SIMP method where the elastic element stiffness matrix with intermediate density is penalized by the corresponding density design variable.[3,57] The main purpose of using Equation (20) is to exclude the superficial buckling caused by the geometric stiffness matrix of thin element without removing any thin element and keeping the connection of nodes unchanged.

To illustrate the singularity phenomenon of the stability constraint, we investigate the buckling load factor of the solution of the same optimization problem in Section 4.1 without global stability constraint. The linear buckling load factor λ^{cr} before removing thin elements is 0.7971, whereas the value after removing thin elements is 238,440.64. This enormous difference demonstrates that global geometrical stiffness matrix of the structure is highly dependent on its thin elements; therefore the accurate value of λ^{cr} cannot be obtained without removing the thin elements that may have superficial member buckling. However, if the geometrical stiffness matrices of the thin elements are penalized using Equation (20), we can eliminate such negative effect in the global stiffness matrix and obtain the accurate value of λ^{cr} without removing the thin elements. Figure 4 shows the relationship between λ^{cr} before removing thin elements and the penalization parameter ρ in Equation (20). The value of λ^{cr} after removing the thin elements is also plotted with red line for comparison. As we can see from Figure 4, the value of λ^{cr} before removing the thin elements increases as ρ is increased, and becomes close to 238440.64 when ρ is greater than 1, indicating that the global stability of the structure can be evaluated by using Equation (20) with a value of ρ larger than 1. Therefore, in this study we choose $\rho = 2$ in Equation (20) to penalize the geometrical stiffness matrix of a thin element.

5 | NUMERICAL EXAMPLES

Three numerical examples are presented in this section to demonstrate the effectiveness of the proposed method. The nonlinear optimization problem (18) is solved using CONOPT in the MATLAB interface of TOMLAB with default settings.[56] As discussed in Section 3.3, since the robustness level β is a decreasing function of order k with given sample size m_{s}, and higher values of β and confidence level α_k lead to a better approximation of the worst structural response, we assume $k = 1$, $m_{\mathrm{s}} = 150$ and $\alpha_k = 0.9995$ for problem (18) in the three examples, that is, the order statistics $\sigma_{k:m_{\mathrm{s}}}$ and $\gamma^{\mathrm{cr}}_{k:m_{\mathrm{s}}}$ in problem (18) are written as $\sigma_{1:150}$ and $\gamma^{\mathrm{cr}}_{1:150}$, respectively, and the corresponding robustness β of both maximum stress and global buckling load factor is 0.95. The eccentricity e for each member in Section 3.1 is 0.01 in accordance with

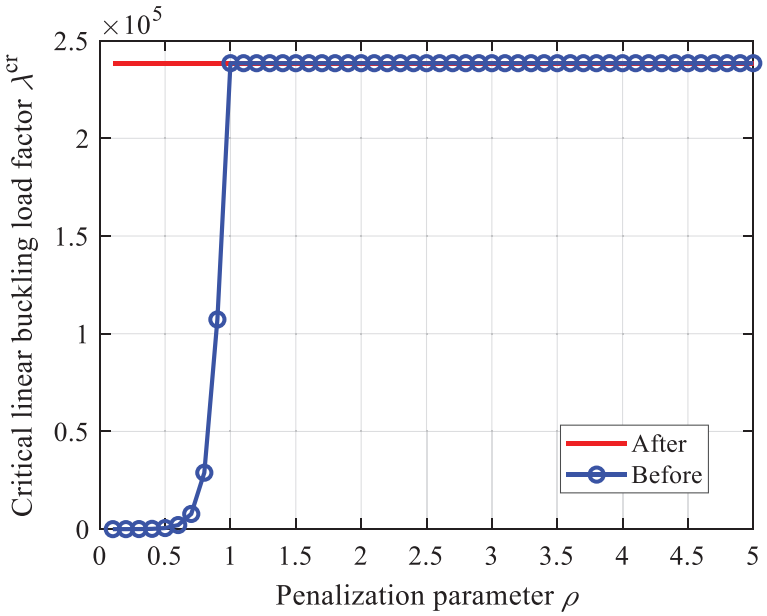

FIGURE 4 Variation of linear buckling load factor with respect to penalization parameter

Reference 58, and the vector $\boldsymbol{\theta} = (\Delta\boldsymbol{x}, \Delta\boldsymbol{y}, \Delta\boldsymbol{A})$ is characterized by uniformly distributed interval variables of the increments indicated by Δ, that is, $\Delta\boldsymbol{x} \in [\Delta\boldsymbol{x}_{\text{lower}}, \Delta\boldsymbol{x}_{\text{upper}}]$, $\Delta\boldsymbol{y} \in [\Delta\boldsymbol{y}_{\text{lower}}, \Delta\boldsymbol{y}_{\text{upper}}]$, $\Delta\boldsymbol{A} \in [\Delta\boldsymbol{A}_{\text{lower}}, \Delta\boldsymbol{A}_{\text{upper}}]$, and $\boldsymbol{\Omega}$ is then defined as $[\Delta\boldsymbol{x}_{\text{lower}}, \Delta\boldsymbol{x}_{\text{upper}}] \times [\Delta\boldsymbol{y}_{\text{lower}}, \Delta\boldsymbol{y}_{\text{upper}}] \times [\Delta\boldsymbol{A}_{\text{lower}}, \Delta\boldsymbol{A}_{\text{upper}}]$, where the subscripts lower and upper represent the lower and upper bounds for the corresponding uncertain parameters, respectively. Note that the same set of uncertain parameters is used at each iteration during optimization process. Validity of this procedure is explained in Appendix A. Because the variation range of uncertain locations of intermediate nodes can be derived with prescribed uncertain nodal locations of free nodes and the eccentricity e, only the bounds for free nodes, denoted by $\Delta\boldsymbol{x}_{\text{free,lower}}$, $\Delta\boldsymbol{x}_{\text{free,upper}}$, $\Delta\boldsymbol{y}_{\text{free,lower}}$, and $\Delta\boldsymbol{y}_{\text{free,upper}}$, are given in each example, and we assume that the nodal uncertainty does not exist in the fixed nodes. The correlated nodal uncertainty values in each member are generated by using copulas[59,60] in MATLAB 2018a[61] and their correlation coefficients calculated by Equation (8). It should be noted that in the formulation of problem (18) no assumption is made on the distribution type of the uncertain parameters; however, in the numerical examples we choose the uniform distribution as the sample-generating mechanism for conveniently constructing the random sample set for order statistics.[43]

Furthermore, since closely spaced nodes may still exist in the optimization process, we hereafter do not divide the frame member if its length is less than 0.1 m; otherwise the frame member is evenly divided into four beam elements as explained in Section 3.1. An element is regarded as thin if its cross-sectional area is less than 1% of the maximum cross-sectional area of the frame. The stress and geometrical stiffness of a thin element are penalized using Equations (19) and (20), respectively. The number of evaluation points p within each element is 6 and their positions are shown in Figure 2(B). The parameter values listed in Table 2 are used in the following numerical examples if not specified explicitly, where $\boldsymbol{t}$ is the vector with all entries equal to 1. Note that $\underline{\boldsymbol{A}}$ in Table 2 is the lower bound of cross-sectional area without considering uncertainty, that is, $\boldsymbol{A} + \Delta\boldsymbol{A} \geq \underline{\boldsymbol{A}}$, and the number of nodes n does not include the intermediate nodes in each member. Flowchart of the proposed method is shown in Figure 5. The deterministic optimization problem (12) is

TABLE 2 Parameter settings of each example

Parameters	Example 1	Example 2	Example 3
Lower bound of $\Delta\boldsymbol{x}_{\text{free,lower}}$ (m)	$-0.02\boldsymbol{t}$	$-0.02\boldsymbol{t}$	$-0.02\boldsymbol{t}$
Upper bound of $\Delta\boldsymbol{x}_{\text{free,upper}}$ (m)	$0.02\boldsymbol{t}$	$0.02\boldsymbol{t}$	$0.02\boldsymbol{t}$
Lower bound of $\Delta\boldsymbol{y}_{\text{free,lower}}$ (m)	$-0.02\boldsymbol{t}$	$-0.02\boldsymbol{t}$	$-0.02\boldsymbol{t}$
Upper bound of $\Delta\boldsymbol{y}_{\text{free,lower}}$ (m)	$0.02\boldsymbol{t}$	$0.02\boldsymbol{t}$	$0.02\boldsymbol{t}$
Lower bound of $\Delta\boldsymbol{A}_{\text{lower}}$ (m^2)	$-0.02\boldsymbol{A}$	$-0.02\boldsymbol{A}$	$-0.02\boldsymbol{A}$
Upper bound of $\Delta\boldsymbol{A}_{\text{upper}}$ (m^2)	$0.02\boldsymbol{A}$	$0.02\boldsymbol{A}$	$0.02\boldsymbol{A}$
Young's modulus $\boldsymbol{E}$ (Pa)	$2\times10^{11}\boldsymbol{t}$	$2\times10^{11}\boldsymbol{t}$	$2\times10^{11}\boldsymbol{t}$
Sample size m_s	150	150	150
k in problem (18)	1	1	1
Confidence level α_k	0.9995	0.9995	0.9995
Robustness β	0.95	0.95	0.95
Upper bound of $\overline{\boldsymbol{A}}$ (m^2)	$0.05\boldsymbol{t}$	$0.05\boldsymbol{t}$	$0.05\boldsymbol{t}$
Lower bound of $\underline{\boldsymbol{A}}$ (m^2)	$1\times10^{-7}\boldsymbol{t}$	$1\times10^{-7}\boldsymbol{t}$	$1\times10^{-7}\boldsymbol{t}$
Upper bound of $\overline{\boldsymbol{q}}$ (N/m)	$1000\boldsymbol{t}$	$1000\boldsymbol{t}$	$1000\boldsymbol{t}$
Lower bound of $\underline{\boldsymbol{q}}$ (N/m)	$-1000\boldsymbol{t}$	$-1000\boldsymbol{t}$	$-1000\boldsymbol{t}$
Upper bound of V_U (m^3)	0.02	0.1	0.1
Lower bound of λ_L	3.4	50	19
Corresponding γ_U	0.29	0.02	0.052
Correlation length L_{exp} (m)	0.1	0.1	0.1
Number of members m	10	27	21
Number of nodes n	6	12	10
Eccentricity e	0.01	0.01	0.01

also solved in each example for comparison purpose, and the solution of robust optimization problem (18) and deterministic optimization problem (12) are denoted as solutions R and D, respectively. Note that the crossing members are not connected at their intersection also in the following examples.

5.1 | Example 1

The first example is a plane frame with two square units, and the initial frame is shown in Figure 6. The frame is pin-supported at nodes 1 and 2, and a downward vertical load $F = 200$ kN is applied at node 5. The fixed nodes are selected as nodes 1, 2 and 5, and the others are free nodes. The robust and deterministic solutions R and D are obtained by solving optimization problems (18) and (12), respectively.

The solutions R and D are shown in Figure 7, where the contour represents the value of von Mises stress. The nodal locations, force densities, cross-sectional areas, and member lengths of solutions R and D are listed in Tables 3 and 4. Note that the stress distributions in Figure 7 are obtained without considering uncertainty in solutions R and D. In order to give a more intuitive comparison, the worst case of stress distributions of solutions R and D are shown in Figure 8, and the values of σ, $\sigma_{1:150}$, γ^{cr}, λ^{cr}, $\gamma^{\mathrm{cr}}_{1:150}$, $\lambda^{\mathrm{cr}}_{1:150}$, and V are also listed in Table 5.

It can be seen from Figure 7 and Table 5 that solution D has a smaller σ than solution R and the linear buckling load factor of solution D is close to λ_{L}. Moreover, for solution D the von Mises stress in the elements with moderate cross-sectional areas are at the similar magnitude and close to σ, which means that the limited material is fully utilized in solution D. However, as we can see from Tables 3 and 4, the cross-sectional areas of members 1 and 6 in solution D

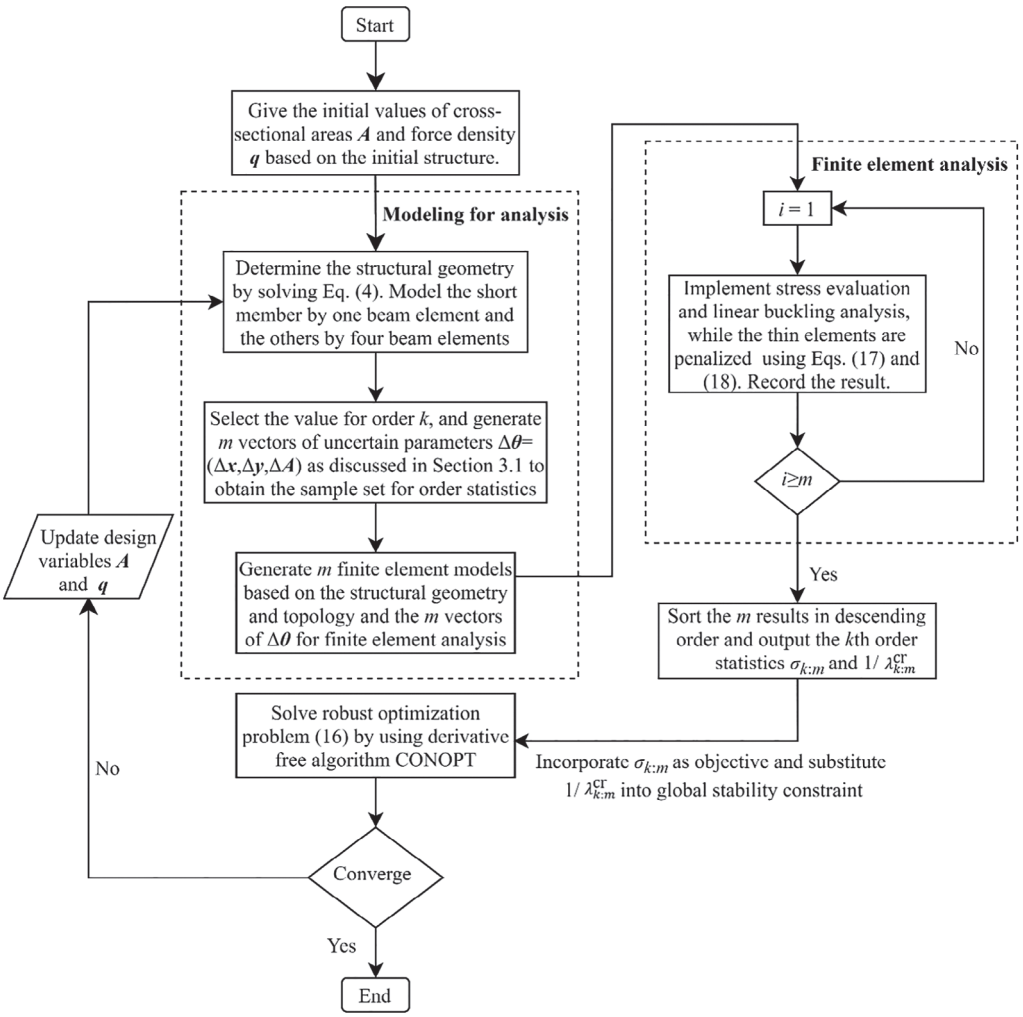

FIGURE 5 Flowchart of robust geometry and topology optimization of plane frame

FIGURE 6 Initial frame of Example 1

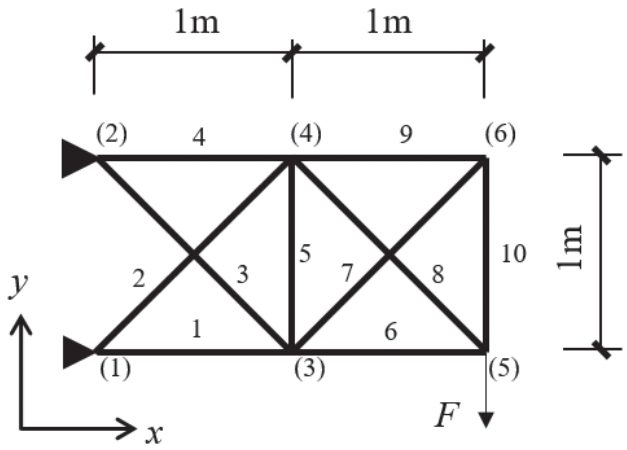

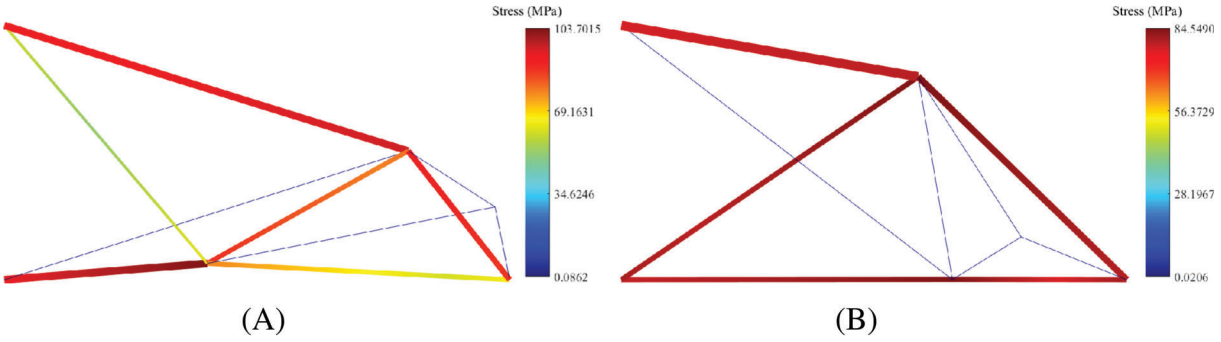

FIGURE 7 Solutions of Example 1 and stress distribution without uncertainty: (A) Solution R; (B) Solution D

TABLE 3 Nodal location of solutions of Example 1

	Solution R		Solution D	
Node number	*x*-coordinate (m)	*y*-coordinate (m)	*x*-coordinate (m)	*y*-coordinate (m)
1	0	0	0	0
2	0	1	0	1
3	0.8011	0.0631	1.3101	0.0008
4	1.6003	0.5087	1.1747	0.7980
5	2	0	2	0
6	1.9439	0.2882	1.5822	0.1685

are almost the same and nodes 1, 3, and 5 are almost located at the same horizontal line; therefore members 1 and 6 can be considered as a long member connecting nodes 1 and 5, resulting in a much higher $\sigma_{1:150}$ and a violation on global stability constraint when uncertainty is involved, which can be seen in Figure 8(B) and Table 5.

While the stress distribution in solution R has several different stress levels and some of these elements have much smaller von Mises stress than σ, the long member in solution D no longer exists in solution R and node 3 is connected by more elements, increasing the redundancy of the structure to reduce the effect of uncertainty on structural performance. In addition, compared to solution D, the overall height of solution R is smaller. It is observed from Figure 8 that at the worst case more elements in solution R have high stress level close to $\sigma_{1:150}$, while in solution D the high stress level only exists in the elements at the bottom, which demonstrates that the elements in solution R cooperate with each other to reduce the maximum stress. Table 5 also indicates that $\sigma_{1:150}$ of solution R is smaller than that of solution D, and the global stability constraint is satisfied under uncertainty which is far from being active. Specifically, $\sigma_{1:150}$ of solution R increases about 126.34% from σ and $\lambda^{\mathrm{cr}}_{1:150}$ decreases about 5.02% from λ^{cr}, whereas $\sigma_{1:150}$

TABLE 4 Cross-sectional area, force density, and member length of solutions of Example 1

	Solution R			Solution D		
Member number	Cross-sectional area (m^2)	Force density (N/m^2)	Length (m)	Cross-sectional area (m^2)	Force density (N/m^2)	Length (m)
1	0.004302	0.2617	0.8059	0.002678	0.4489	1.3101
2	1×10^{-7}	0.0933	1.6767	0.002933	−0.4132	1.4202
3	0.001560	0.1924	1.2332	1×10^{-7}	−0.1647	1.6476
4	0.004069	0.1263	1.6729	0.005220	0.7074	1.1920
5	0.002682	−0.2225	0.9096	1×10^{-7}	0.0980	0.8085
6	0.002719	0.5726	1.1983	0.002675	0.3539	0.6898
7	1×10^{-7}	−0.1260	1.1603	1×10^{-7}	0.5198	0.3196
8	0.003228	0.0078	0.6462	0.003710	0.2497	1.1480
9	1×10^{-7}	0.4978	0.4081	1×10^{-7}	0.3099	0.7499
10	1×10^{-7}	0.4798	0.2921	1×10^{-7}	0.6410	0.4504

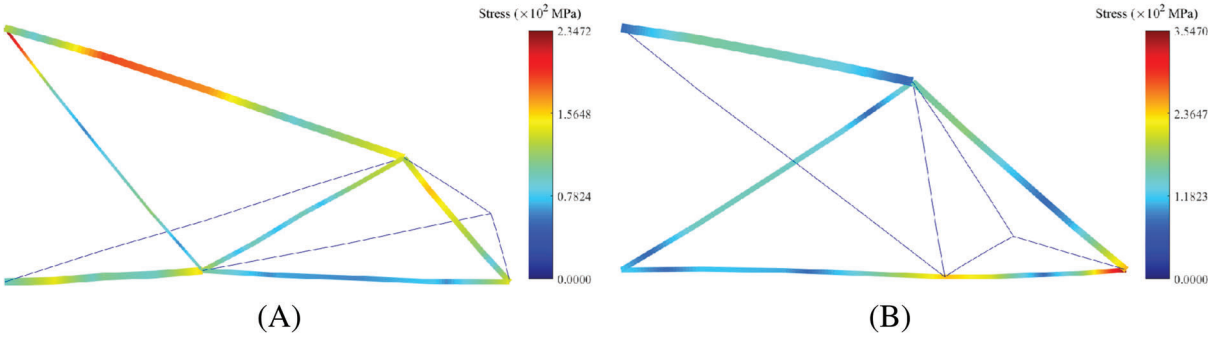

FIGURE 8 Solutions of Example 1 and worst stress distribution: (A) Solution R; (B) Solution D

TABLE 5 Values of σ, $\sigma_{1:150}$, γ^{cr}, λ^{cr}, $\gamma^{cr}_{1:150}$, $\lambda^{cr}_{1:150}$, and V of solutions of Example 1

Solution	σ (MPa)	$\sigma_{1:150}$ (MPa)	γ^{cr}	λ^{cr}	$\gamma^{cr}_{1:150}$	$\lambda^{cr}_{1:150}$	V (m^3)
R	103.7015	234.7208	0.0868	11.5117	0.0914	10.9328	0.02
D	84.5490	354.7003	0.2899	3.4490	0.3193	3.1314	0.02

of solution D increases about 319.52% from σ and $\lambda^{cr}_{1:150}$ decreases about 9.02% from λ^{cr}. This result indicates that solution R is more robust and stable than solution D with respect to reducing the influence of uncertainty in nodal locations and cross-sectional areas on structural performance. Although the details are not shown, a similar solution as solution D is obtained if global stability constraint is not considered. This fact emphasizes the importance of the proposed penalization method of the geometric stiffness matrix to obtain the optimal solution neglecting the superficial buckling of the thin members.

Furthermore, the iteration histories of values of uncertainties in the x-coordinate of node 3 and y-coordinate of node 4, denoted by Δx_3 and Δy_4, respectively, and cross-sectional areas of members 1 and 4, denoted by ΔA_1 and ΔA_4, respectively, in the worst case scenario are presented in Figure 9(A), and the iteration history of $\sigma_{1:150}$ is also presented in Figure 9(B). Note that for simplicity in Figure 9(A) only the values of every 10 iterations are shown. It can be observed from Figure 9(A) that the values of uncertainties in nodal coordinates and cross-sectional areas in the worst case scenario change during the optimization procedure, indicating that the worst case scenarios would switch with respect to the variations of uncertain parameters. Moreover, in Figure 9(B) there are several humps in the iteration history of $\sigma_{1:150}$ which increase rapidly to a very large value. The main reason for this would be that since the optimization problem is nonlinear with respect to

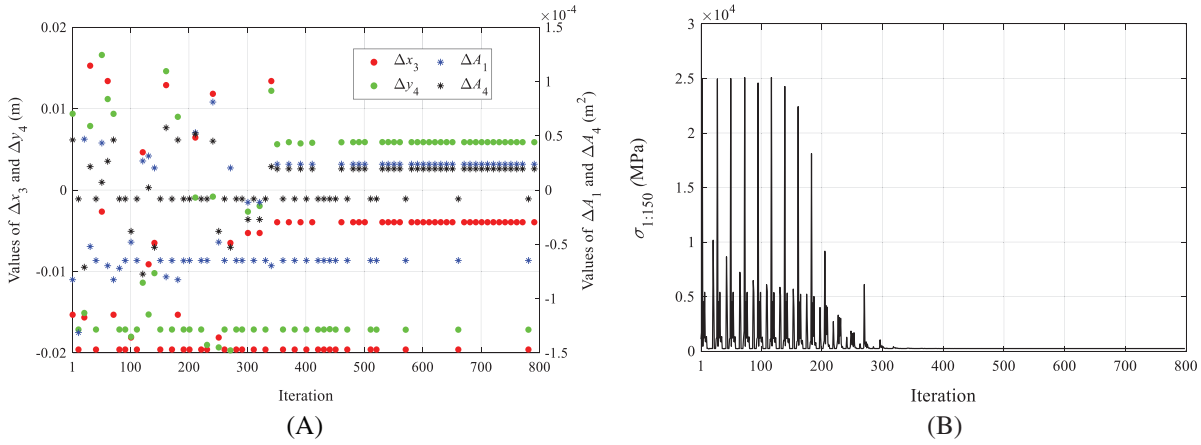

FIGURE 9 Iteration history of Example 1: (A) Values of Δx_3, Δy_4, $\Delta A_1$and ΔA_4 in worst case scenario; (B) first order statistic $\sigma_{1:150}$

FIGURE 10 Initial frame of Example 2

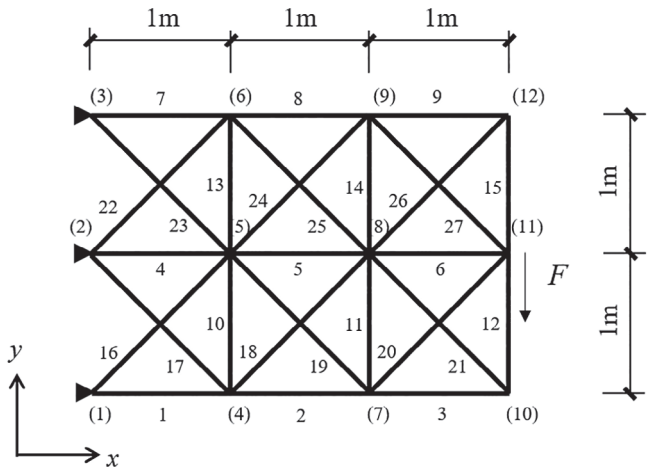

the design variables, solutions that are sensitive to uncertain parameters are sometimes evaluated during optimization, resulting in a large value of $\sigma_{1:150}$. However, in this example the values of humps are gradually decreased and the worst case scenario converged as the optimization procedure converged to a local minimum with an appropriate shape and topology. In addition, we further investigate the effect of using different sampling sets for constructing the order statistics on final design, and the results are presented in Appendix A.

5.2 | Example 2

The second example is another cantilever beam plane frame structure with 3×2 units. The structure is pin-supported at nodes 1, 2, and 3, and a downward vertical load $F = 100$ kN is applied at node 11 as shown in Figure 10.

In a similar manner as Example 1, we solve both the robust and deterministic optimization problems (18) and (12) for Example 2. The nodal locations, cross-sectional areas, force densities, and member lengths of solutions R and D are listed in Tables 6 and 7, and Table 8 lists the values of σ, $\sigma_{1:150}$, γ^{cr}, λ^{cr}, $\gamma^{\text{cr}}_{1:150}$, $\lambda^{\text{cr}}_{1:150}$, and V. Solutions R and D are shown in Figure 10 and the stress contours are obtained without considering uncertainty, while Figure 11 shows the worst stress distributions of solutions R and D. It should be noted that since the stress of short members are ignored during the optimization, the stresses of short member 6 in solution R and short members 1 and 7 in solution D are represented as 0 in Figures 11 and 12.

It can be seen from Figure 11 and Tables 6 and 7 that compared to solution D, the nodal locations and cross-sectional areas of solution R are asymmetric with respect to the x-axis, and σ of solution R is almost twice of solution D. However, when uncertainty is added to the nodal locations and cross-sectional areas, $\sigma_{1:150}$ of solution D significantly increases

TABLE 6 Nodal location of solutions of Example 2

	Solution R		Solution D	
Node number	*x*-coordinate (m)	*y*-coordinate (m)	*x*-coordinate (m)	*y*-coordinate (m)
1	0	0	0	0
2	0	1	0	1
3	0	2	0	2
4	0.9342	0.1628	0.0249	0.0060
5	1.4275	1.0654	1.3000	1.0004
6	0.6667	1.9573	0.0250	1.9939
7	1.9891	0.3623	1.8630	0.2935
8	2.9738	0.8939	1.4999	1.0004
9	1.8244	1.8063	1.8622	1.7067
10	2.7641	1.2496	2.7868	1.2748
11	3	1	3	1
12	2.8315	1.0208	2.2953	1.9169

TABLE 7 Cross-sectional area and force density of solutions of Example 2

	Solution R			Solution D		
Member number	Cross-sectional area (m^2)	Force density (N/m^2)	Length (m)	Cross-sectional area (m^2)	Force density (N/m^2)	Length (m)
1	0.0077	0.8088	0.9483	0.0099	0.0114	0.0257
2	0.0064	−0.8207	1.0735	0.0114	0.0659	1.8603
3	5.52×10^{-7}	0.0845	1.1781	1×10^{-7}	−0.0595	1.3477
4	1.87×10^{-7}	−0.0556	1.4290	1×10^{-7}	0.07949	1.3000
5	1.83×10^{-7}	0.0867	1.5557	1×10^{-7}	−0.4249	0.1999
6	9.49×10^{-7}	−0.9537	0.1000	1×10^{-7}	−0.4484	1.5000
7	0.0077	1.3707	0.6681	0.0099	0.0383	0.0257
8	0.0064	0.0208	1.1674	0.0113	0.2297	1.8595
9	1.85×10^{-7}	0.0864	1.2772	1×10^{-7}	−0.1393	0.4814
10	0.0056	0.5636	1.0286	1×10^{-7}	0.1459	1.6169
11	3.51×10^{-6}	−0.8759	1.1191	0.0017	−0.1890	0.7946
12	2.99×10^{-7}	1.2386	0.3434	1×10^{-7}	0.1458	0.3478
13	0.0054	1.1569	1.1722	1×10^{-7}	−0.0752	1.6164
14	1.84×10^{-7}	0.4991	1.4675	0.0017	−0.2745	0.7937
15	1.84×10^{-7}	0.0748	0.1697	1×10^{-7}	−0.0232	1.1564
16	0.0061	−0.1373	1.7813	0.0036	−0.2397	1.6403
17	0.0032	−0.5928	1.2544	1×10^{-7}	0.0424	0.9943
18	1.86×10^{-7}	0.3870	2.1667	0.0028	−0.2074	1.7789
19	0.0036	0.2556	0.8998	0.0028	0.1364	0.9036
20	0.0098	0.0740	1.1952	0.0103	0.1622	1.3385
21	1.78×10^{-7}	−1.0804	0.4129	1×10^{-7}	0.0669	1.3158
22	0.0031	−0.7756	1.1666	1×10^{-7}	0.2256	0.9943
23	0.0061	−0.4466	1.7062	0.0036	0.0815	1.6398
24	0.0039	−0.0823	0.8404	0.0028	−0.0069	0.9027
25	1.85×10^{-7}	−0.2199	2.5403	0.0028	−0.2167	1.7783
26	1.83×10^{-7}	0.5229	0.1906	1×10^{-7}	0.0552	1.2134
27	0.0098	−0.5693	1.4255	0.0102	0.3332	1.3393

TABLE 8 Values of σ, $\sigma_{1:150}$, γ^{cr}, λ^{cr}, $\gamma^{cr}_{1:150}$, $\lambda^{cr}_{1:150}$, and V of solutions of Example 2 before merging the closely spaced nodes and removing thin elements

Solution	σ (MPa)	$\sigma_{1:150}$ (MPa)	γ^{cr}	λ^{cr}	$\gamma^{cr}_{1:150}$	$\lambda^{cr}_{1:150}$	V (m^3)
R	16.6915	28.7047	0.0102	97.9790	0.0107	92.7861	0.1
D	9.7051	38.1419	0.0195	51.1818	0.0216	47.2584	0.1

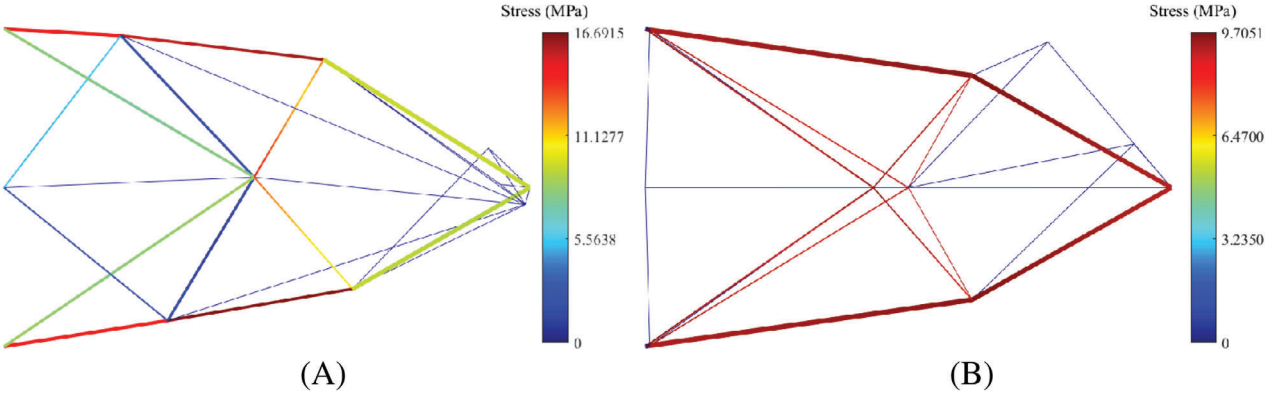

FIGURE 11 Solutions of Example 2 and stress distribution without uncertainty: (A) Solution R; (B) Solution D

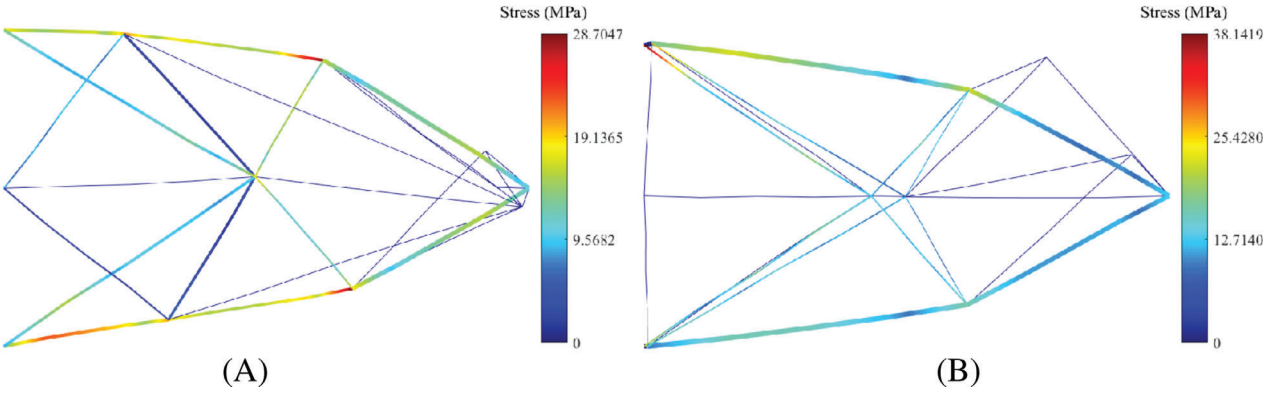

FIGURE 12 Solutions of Example 2 and worst stress distribution: (A) Solution R; (B) Solution D

about 293% from 9.7051 to 38.1419 MPa, and $\lambda^{cr}_{1:150}$ is also decreases about 7.67% from λ^{cr} which violates the global stability constraint. This is mainly because the existence of long members in solution D makes the structure more sensitive to the asymmetric uncertainty. By contrast, $\sigma_{1:150}$ of solution R is smaller than that of solution D as more members have increased their cross-sectional areas and connect to the support node 2, avoiding the existence of long members and increasing the structural stability. In addition, we can see from Table 7 that $\lambda^{cr}_{1:150}$ of solution R decreases only about 5.3% from λ^{cr} and the global stability constraint is also satisfied under uncertainty, which indicates solution R is has more stability than solution D.

Figures 13 and 14 show the stress contours of solutions R and D without considering uncertainty and the corresponding worst stress distributions, respectively, after merging the closely spaced nodes and removing thin elements. The values of σ, $\sigma_{1:150}$, γ^{cr}, λ^{cr}, $\gamma^{cr}_{1:150}$, $\lambda^{cr}_{1:150}$, and V of solutions in Figures 13 and 14 are listed in Table 9. It can be found that the differences of Tables 8 and 9 for solutions R and D are about 1.5% or less, however, as stated in Section 3.3, unexpectedly large stress might exist in a short member with moderate cross-sectional area due to its large bending stiffness, and would provide an inaccurate stress to be minimized if it is considered during optimization procedure. For example, the von Mises stress of members 1 and 7 without uncertainty in solution D are both

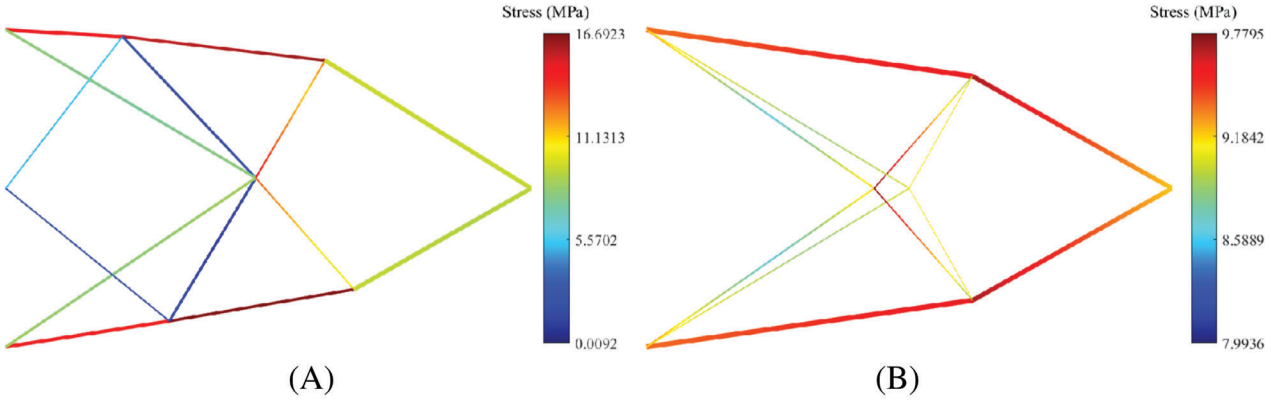

FIGURE 13 Solutions of Example 2 and stress distribution without uncertainty after merging the closely spaced nodes and removing thin elements: (A) Solution R; (B) Solution D

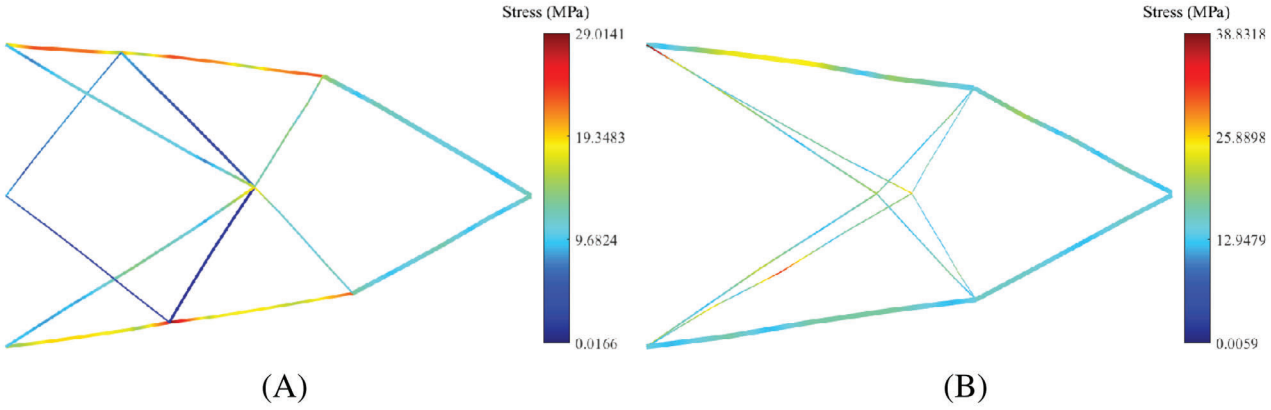

FIGURE 14 Solutions of Example 2 and worst stress distribution after merging the closely spaced nodes and removing thin elements: (A) Solution R; (B) Solution D

TABLE 9 Values of σ, $\sigma_{1:150}$, γ^{cr}, λ^{cr}, $\gamma^{cr}_{1:150}$, $\lambda^{cr}_{1:150}$, and V of solutions of Example 2 after merging the closely spaced nodes and removing thin elements

Solution	σ (MPa)	$\sigma_{1:150}$ (MPa)	γ^{cr}	λ^{cr}	$\gamma^{cr}_{1:150}$	$\lambda^{cr}_{1:150}$	V (m^3)
R	16.6923	29.0141	0.0102	97.9778	0.0108	92.2404	0.1
D	9.7795	38.8318	0.0197	50.7112	0.0211	47.4364	0.1

13.0781 MPa, which is much larger than the stress after merging the closely spaced nodes and removing thin elements. Therefore, the stress in short member is set to 0 during the optimization procedure to avoid such inaccurate stress to be minimized.

It can be seen from Tables 6-8 that solutions R and D have the same structural volume that is equal to its upper bound; however, they have different structural geometries and distributions of cross-sectional areas, leading to a trade-off relationship between structural robustness and performance. Specifically, solution D is more vulnerable to uncertainty which has a smaller structural stress with satisfied global stability constraint at deterministic conditions, while solution R is a much more stable and robust structure with larger stress for the nominal values of the uncertain parameters.

5.3 | Example 3

In the last example we investigate the robust optimization problem of a bridge frame with 4×1 units. The initial ground structure is shown in Figure 15. The frame is pin-supported at node 1 and roller supported at node 9, and three downward vertical loads $F = 100$ kN are applied at nodes 3, 5, and 7. Accordingly, these five nodes are regarded as fixed nodes during the optimization procedure. In order to present the solution which degenerates into a line between the supports, the locations of free nodes are obtained using reaction forces at supports as suggested in Reference 13.

In this example the free nodes 2, 4, 6, 8, and 10 are only allowed to move in the y-direction. The robust and deterministic optimization problems (18) and (12) are solved, and solutions R and D and their stress contours are shown in Figure 15. The corresponding worst stress distributions are shown in Figure 15. Tables 10 and 11 list the nodal locations, force densities, cross-sectional areas and member lengths of solutions R and D, and the corresponding values of σ, $\sigma_{1:150}$, γ^{cr}, λ^{cr}, $\gamma^{\mathrm{cr}}_{1:150}$, $\lambda^{\mathrm{cr}}_{1:150}$, and V are listed in Table 12.

It can be seen from Figure 16 and Table 11 that because the cross-sectional areas of members 2 and 17 are small, solution D is unstable in x-direction if the bending stiffness is small, and therefore the worst stress increases rapidly when uncertainty is taken into consideration. The worst maximum stress of solution D exists at the brace member 13 as shown in Figure 17, while other members are at relatively low stress level and make little contribution to reducing the effect of uncertainty. The global stability constraint of solution D is also violated when uncertainty is considered, and $\lambda^{\mathrm{cr}}_{1:150}$ decreases about 8.6% from λ^{cr}. On the other hand, solution R has a different geometry and topology from solution R in which the cross-sectional areas of members 2, 8, 14, and 17 are increased, leading to a more stable structure with larger value of λ^{cr}. Moreover, we can observe from Figure 17 that since more members have larger cross-sectional areas, solution R is able to work better than solution D as a whole to resist external force under uncertainty; therefore, the large stress appears at several different elements, and the global stability constraint is also satisfied with small decrease of $\lambda^{\mathrm{cr}}_{1:150}$.

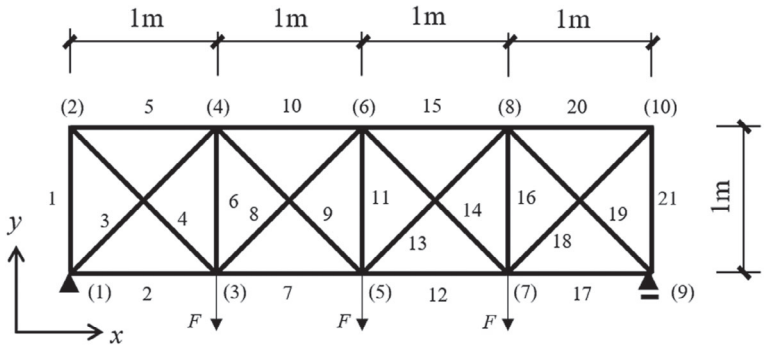

FIGURE 15 Initial frame of Example 3

TABLE 10 Nodal location of solutions of Example 3

	Solution R		Solution D	
Node number	***x*-coordinate (m)**	***y*-coordinate (m)**	***x*-coordinate (m)**	***y*-coordinate (m)**
1	0	0	0	0
2	0	0.808689	0	0.6246
3	1	0	1	0
4	1	1.208606	1	1.4526
5	2	0	2	0
6	2	1.53403	2	1.7311
7	3	0	3	0
8	3	1.244731	3	1.4527
9	4	0	4	0
10	4	0.639194	4	0.6237

TABLE 11 Cross-sectional area and force density of solutions of Example 3

	Solution R			Solution D		
Member number	Cross-sectional area (m^2)	Force density (N/m^2)	Length (m)	Cross-sectional area (m^2)	Force density (N/m^2)	Length (m)
1	6.93×10^{-7}	10.2065	1.0086	0.0096	29.6315	0.8245
2	0.00642865	4.7562	1	1×10^{-7}	−0.2321	1
3	0.0097405	−113.7971	1.7274	1×10^{-7}	−105.5527	1.9315
4	7.33×10^{-7}	−59.1720	1.4203	0.0075	−93.2228	1.2961
5	7.42×10^{-7}	−41.1605	1.0770	0.0075	−0.2160	1.2983
6	0.0058	229.7475	1.4086	0.0016	77.7386	1.6525
7	0.0059	−49.7649	1	0.0058	0.07071	1
8	8.53×10^{-4}	−94.5413	2.0017	1×10^{-7}	25.0637	2.1746
9	0.0019	194.7562	1.7274	0.0015	123.7339	1.9315
10	0.0068	11.9206	1.0516	0.0069	−0.0105	1.0380
11	0.0045	1.8782	1.7340	0.0037	−114.7634	1.9310
12	0.0058	28.6246	1	0.0058	0.2714	1
13	0.0020	−122.9237	1.7570	0.0016	70.8772	1.9316
14	1.77×10^{-4}	55.6022	2.0017	1×10^{-7}	−34.6783	2.1746
15	0.0064	−19.8246	1.0410	0.0069	0.2533	1.0380
16	0.0068	−286.7470	1.4447	0.0016	59.8102	1.6526
17	0.0066	26.1264	1	1×10^{-7}	−0.1531	1
18	6.75×10^{-7}	497.9256	1.3054	0.0075	82.6981	1.2955
19	0.0101	368.3595	1.7570	1×10^{-7}	−50.7874	1.9316
20	6.75×10^{-7}	−46.5193	1.1690	0.0075	0.3086	1.2989
21	5.52×10^{-7}	−812.8990	0.8391	0.0096	−80.2037	0.8237

TABLE 12 Values of σ, $\sigma_{1:150}$, γ^{cr}, λ^{cr}, $\gamma^{cr}_{1:150}$, $\lambda^{cr}_{1:150}$, and V of solutions of Example 3

Solution	σ (MPa)	$\sigma_{1:150}$ (MPa)	γ^{cr}	λ^{cr}	$\gamma^{cr}_{1:150}$	$\lambda^{cr}_{1:150}$	V (m^3)
R	24.9122	42.3885	0.0176	56.6598	0.0186	53.5824	0.1
D	18.0690	70.8619	0.0514	19.4295	0.0558	17.8929	0.1

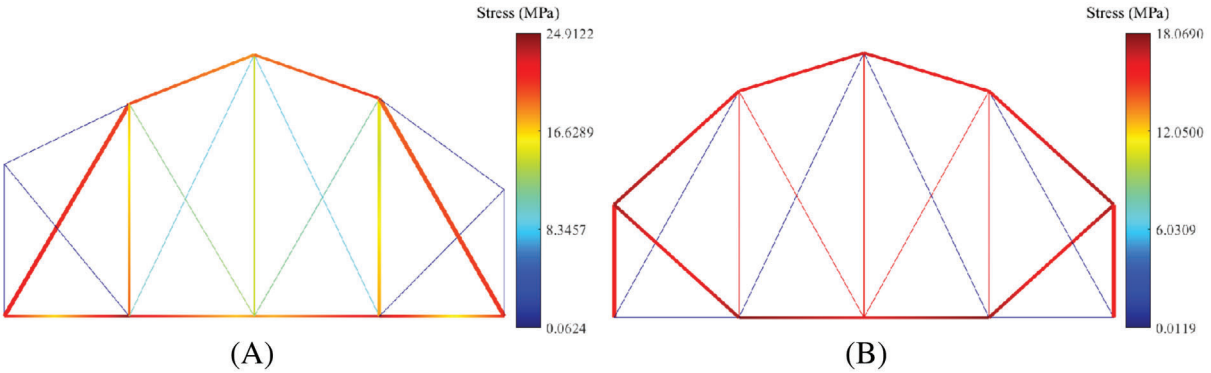

FIGURE 16 Solutions of Example 3 and stress distribution without uncertainty: (A) Solution R; (B) Solution D

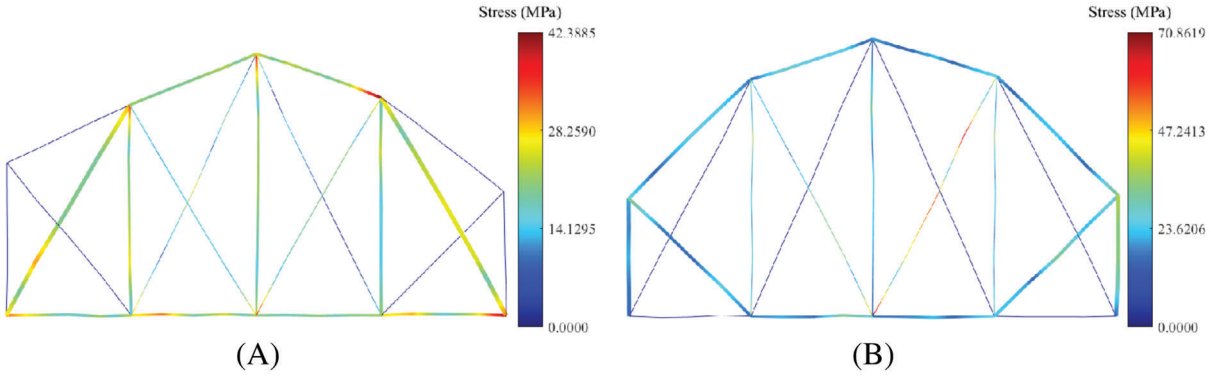

FIGURE 17 Solutions of Example 3 and worst stress distribution: (A) Solution R; (B) Solution D

Again, it can be also observed from Table 12 that both solutions R and D have the same structural volume, however, their structural performance depends on the consideration of uncertainty, indicating a trade-off relationship between the robustness and the structural performance represented by stress and critical linear buckling load factor.

6 | CONCLUSION

A worst case approach has been presented for robust simultaneous geometry and topology optimization of plane frames to minimize the maximum von Mises stress under volume and global stability constraints. An auxiliary truss to which the FDM is applied is used to define the geometry of the frame, and the difficulty due to the existence of melting nodes is prevented by limiting the force density of each member to indirectly control the member length. The problem is converted into an RDO problem with semi-infinite constraints, and uncertainty is represented by the random variations in nodal locations and in cross-sectional areas without any assumption on their distribution information. The exact worst values of the maximum stress and the global buckling load factor are relaxed to the quantile responses. The order statistics is employed to approximate the relaxed quantile response, and the robustness is indicated by the order k with specified sample size and confidence level. A robust optimization problem of plane frame is formulated with respect to the force densities and cross-sectional areas under constraints on structural volume and the smallest positive linear buckling load factor under uncertainty.

The stress of a thin element is penalized to underestimate its value with respect to the cross-sectional area, and the penalization method is extended to underestimate the geometrical stiffness matrix of the thin elements. A simple example to minimize the maximum stress without considering uncertainty is presented to confirm the effectiveness of the proposed numerical penalization method.

Three numerical examples are presented to investigate the effectiveness of the proposed method, and in each example a deterministic optimization problem is also solved for comparison purpose. Both optimization problems are solved using the GRG method available in the library CONOPT with MATLAB interface. It is shown that the solutions of deterministic and robust optimization problems have different geometries and topologies, leading to different performance on minimizing the maximum stress and satisfying the global stability constraint. While the solution of robust optimization contains some elements which are not effective to minimize the stress without considering uncertainty, it is helpful to reduce the worst value of stress and increase the global buckling load factor, resulting in a structure less sensitive to the uncertainty.

It is interesting to note that in the second example the closely spaced nodes appear and unexpectedly large stress exists in the short member due to its large bending stiffness if the cross-sectional area is not small. Such large stress in a short member is set to 0 during the optimization procedure to provide an accurate stress to be minimized. The results confirm that the differences of structural responses of the solutions before and after merging the closely spaced nodes and removing the thin elements are sufficiently small.

ACKNOWLEDGMENT

This research is partially supported by China Scholarship Council (File No. 201806050114).

DATA AVAILABILITY STATEMENT

The data that support the findings of this study are available from the corresponding author upon reasonable request.

ORCID

Wei Shen https://orcid.org/0000-0003-2616-7741

REFERENCES

1. Stolpe M. Truss optimization with discrete design variables: a critical review. *Struct Multidiscip Optim*. 2016;53(2):349-374. https://doi.org/10.1007/s00158-015-1333-x.
2. Arora JS, Wang Q. Review of formulations for structural and mechanical system optimization. *Struct Multidiscip Optim*. 2005;30(4):251-272. https://doi.org/10.1007/s00158-004-0509-6.
3. Bendsøe MP, Sigmund O. *Topology Optimization: Theory, Methods, and Applications*. New York, NY: Springer; 2003.
4. Ohsaki M. *Optimization of Finite Dimensional Structures*. Boca Raton, FL: CRC Press; 2010.
5. Dorn WS, Gomory RE, Greenberg HJ. Automatic design of optimal structures. *J Mech*. 1964;3:25-52.
6. Gil L, Andreu A. Shape and cross-section optimization of a truss structure. *Comput Struct*. 2001;79(7):681-689. https://doi.org/10.1016/S0045-7949(00)00182-6.
7. Achtziger W. On simultaneous optimization of truss geometry and topology. *Struct Multidiscip Optim*. 2007;33(4–5):285-304. https://doi.org/10.1007/s00158-006-0092-0.
8. Ohsaki M. Simultaneous optimization of topology and geometry of a regular plane truss. *Comput Struct*. 1998;66(1):69-77. https://doi.org/10.1016/S0045-7949(97)00050-3.
9. Wang D, Zhang WH, Jiang JS. Combined shape and sizing optimization of truss structures. *Comput Mech*. 2002;29(4–5):307-312. https://doi.org/10.1007/s00466-002-0343-x.
10. Wang D, Zhang WH, Jiang JS. Truss shape optimization with multiple displacement constraints. *Comput Methods Appl Mech Eng*. 2002;191(33):3597-3612. https://doi.org/10.1016/S0045-7825(02)00297-9.
11. Ohsaki M, Hayashi K. Force density method for simultaneous optimization of geometry and topology of trusses. *Struct Multidiscip Optim*. 2017;56(5):1157-1168. https://doi.org/10.1007/s00158-017-1710-8.
12. Hayashi K, Ohsaki M. FDMopt: force density method for optimal geometry and topology of trusses. *Adv Eng Softw*. 2019;133:12-19. https://doi.org/10.1016/j.advengsoft.2019.04.002.
13. Shen W, Ohsaki M. Geometry and topology optimization of plane frames for compliance minimization using force density method for geometry model. *Eng Comput*. 2020. https://doi.org/10.1007/s00366-019-00923-w.
14. Rozvany GIN. Difficulties in truss topology optimization with stress, local buckling and system stability constraints. *Struct Optim*. 1996;11(3–4):213-217. https://doi.org/10.1007/BF01197036.
15. Zhou M. Difficulties in truss topology optimization with stress and local buckling constraints. *Struct Optim*. 1996;11(2):134-136. https://doi.org/10.1007/BF01376857.
16. Ohsaki M, Ikeda K. *Stability and optimization of structures: Generalized Sensitivity Analysis*. Sendai: Springer; 2010.
17. Tugilimana A, Filomeno Coelho R, Thrall AP. Including global stability in truss layout optimization for the conceptual design of large-scale applications. *Struct Multidiscip Optim*. 2018;57(3):1213-1232. https://doi.org/10.1007/s00158-017-1805-2.
18. Ohsaki M, Kanno Y. Optimum design of finite dimensional systems with coincident critical points. Paper presented at: Proceedings of the 4th World Congress of Structural Multidisciplinary Optimisation. (WCSMO4); 2001; Dalian, China.
19. Kanno Y, Ohsaki M, Katoh N. Sequential semidefinite programming for optimization of framed structures under multimodal buckling constraints. *Int J Struct Stab Dyn*. 2001;1(4):585-602.
20. Guo X, Cheng G, Yamazaki K. A new approach for the solution of singular optima in truss topology optimization with stress and local buckling constraints. *Struct Multidiscip Optim*. 2001;22(5):364-372. https://doi.org/10.1007/s00158-001-0156-0.
21. Guo X, Cheng GD, Olhoff N. Optimum design of truss topology under buckling constraints. *Struct Multidiscip Optim*. 2005;30(3):169-180. https://doi.org/10.1007/s00158-004-0511-z.
22. Descamps B, Filomeno CR. The nominal force method for truss geometry and topology optimization incorporating stability considerations. *Int J Solids Struct*. 2014;51(13):2390-2399. https://doi.org/10.1016/j.ijsolstr.2014.03.003.
23. Torii AJ, Lopez RH, Miguel LFF. Modeling of global and local stability in optimization of truss-like structures using frame elements. *Struct Multidiscip Optim*. 2015;51(6):1187-1198. https://doi.org/10.1007/s00158-014-1203-y.
24. Madah H, Amir O. Truss optimization with buckling considerations using geometrically nonlinear beam modeling. *Comput Struct*. 2017;192:233-247. https://doi.org/10.1016/j.compstruc.2017.07.023.
25. Choi S-K, Grandhi RV, Canfield RA. *Reliability-Based Structural Design*. New York, NY: Spinger; 2007.
26. Ben-Tal A, El Ghaoui L, Nemirovski A. *Robust Optimization*. Princeton, NJ: Princeton University Press; 2009.
27. Elishakoff I, Ohsaki M. *Optimization and Anti-Optimization of Structures under Uncertainty*. London, UK: World Scientific; 2010.
28. Asadpoure A, Tootkaboni M, Guest JK. Robust topology optimization of structures with uncertainties in stiffness - application to truss structures. *Comput Struct*. 2011;89(11–12):1131-1141. https://doi.org/10.1016/j.compstruc.2010.11.004.
29. Kang Z, Liu P. Reliability-based topology optimization against geometric imperfections with random threshold model. *Int J Numer Methods Eng*. 2018;115(1):99-116. https://doi.org/10.1002/nme.5797.

30. Mogami K, Nishiwaki S, Izui K, Yoshimura M, Kogiso N. Reliability-based structural optimization of frame structures for multiple failure criteria using topology optimization techniques. *Struct Multidiscip Optim*. 2006;32(4):299-311. https://doi.org/10.1007/s00158-006-0039-5.
31. Guest JK, Igusa T. Structural optimization under uncertain loads and nodal locations. *Comput Methods Appl Mech Eng*. 2008;198(1):116-124. https://doi.org/10.1016/j.cma.2008.04.009.
32. Doltsinis I, Kang Z. Robust design of structures using optimization methods. *Comput Methods Appl Mech Eng*. 2004;193(23–26):2221-2237. https://doi.org/10.1016/j.cma.2003.12.055.
33. Picheny V, Kim NH, Haftka RT. Application of bootstrap method in conservative estimation of reliability with limited samples. *Struct Multidiscip Optim*. 2010;41(2):205-217. https://doi.org/10.1007/s00158-009-0419-8.
34. Thore CJ, Holmberg E, Klarbring A. A general framework for robust topology optimization under load-uncertainty including stress constraints. *Comput Methods Appl Mech Eng*. 2017;319:1-18. https://doi.org/10.1016/j.cma.2017.02.015.
35. Kanno Y, Takewaki I. Confidence ellipsoids for static response of trusses with load and structural uncertainties. *Comput Methods Appl Mech Eng*. 2006;196(1–3):393-403. https://doi.org/10.1016/j.cma.2006.04.007.
36. Kanno Y, Takewaki I. Sequential semidefinite program for maximum robustness design of structures under load uncertainty. *J Optim Theory Appl*. 2006;130(2):265-287. https://doi.org/10.1007/s10957-006-9102-z.
37. Guo X, Bai W, Zhang W, Gao X. Confidence structural robust design and optimization under stiffness and load uncertainties. *Comput Methods Appl Mech Eng*. 2009;198(41–44):3378-3399. https://doi.org/10.1016/j.cma.2009.06.018.
38. Kanno Y, Xu G. A mixed integer programming for robust truss topology optimization with stress constraints Yoshihiro. *Int J Numer Methods Eng*. 2010;83:1675-1699. https://doi.org/10.1002/nme.
39. Fu Z, Wang C, Zhao J. Truss topology optimization under uncertain nodal locations with proportional topology optimization method. *Mech Based Des Struct Mach*. 2017;45(2):190-206. https://doi.org/10.1080/15397734.2016.1163640.
40. Shen W, Ohsaki M, Yamakawa M. Multiobjective robust shape and topology optimization of plane frames using order statistics. *Struct Multidiscip Optim*. 2020;63:75-94. https://doi.org/10.1007/s00158-020-02663-8.
41. Ohsaki M, Yamakawa M, Fan W, Li Z. An order statistics approach to multiobjective structural optimization considering robustness and confidence of responses. *Mech Res Commun*. 2019;97:33-38. https://doi.org/10.1016/j.mechrescom.2019.04.003.
42. Yamakawa M, Ohsaki M. Robust design optimization considering parameter variation of seismic characteristics using order statistics. *J Struct Eng*. 2016;62B:381-388.
43. Rocchetta R, Crespo LG, Kenny SP. A scenario optimization approach to reliability-based design. *Reliab Eng Syst Saf*. 2020;196(July 2019):106755. https://doi.org/10.1016/j.ress.2019.106755.
44. Zhang JY, Ohsaki M. Adaptive force density method for form-finding problem of tensegrity structures. *Int J Solids Struct*. 2006;43(18–19):5658-5673.
45. Kanno Y, Ohsaki M. Minimum principle of complementary energy of cable networks by using second-order cone programming. *Int J Solids Struct*. 2003;40(17):4437-4460. https://doi.org/10.1016/S0020-7683(03)00215-4.
46. Jalalpour M, Guest JK, Igusa T. Reliability-based topology optimization of trusses with stochastic stiffness. *Struct Saf*. 2013;43:41-49. https://doi.org/10.1016/j.strusafe.2013.02.003.
47. Changizi N, Kaboodanian H, Jalalpour M. Stress-based topology optimization of frame structures under geometric uncertainty. *Comput Methods Appl Mech Eng*. 2017;315:121-140. https://doi.org/10.1016/j.cma.2016.10.039.
48. McGuire W, Gallagher RH, Ziemian RD. *Matrix Structural Analysis*. Hoboken, NJ: John Wiley; 2000.
49. Prescott P, Arnold BC, Balakrishnan N, Nagaraja HN. *A First Course in Order Statistics*. Philadelphia: Society for Industrial and Applied Mathematics; 1993.
50. Beyer HG, Sendhoff B. Robust optimization – a comprehensive survey. *Comput Methods Appl Mech Eng*. 2007;196(33–34):3190-3218. https://doi.org/10.1016/j.cma.2007.03.003.
51. Ito M, Kim NH, Kogiso N. Conservative reliability index for epistemic uncertainty in reliability-based design optimization. *Struct Multidiscip Optim*. 2018;57(5):1919-1935. https://doi.org/10.1007/s00158-018-1903-9.
52. Moon M, Cho H, Choi KK, Lamb D. Confidence-based reliability assessment considering limited numbers of both input and output test data. *Struct Multidiscip Optim*. 2018;57:2027-2043.
53. Kanno Y. A data-driven approach to non-parametric reliability-based design optimization of structures with uncertain load. *Struct Multidiscip Optim*. 2019;60:83-97. https://doi.org/10.1007/s00158-019-02199-6.
54. Gabrel V, Murat C, Thiele A. Recent advances in robust optimization: an overview. *Eur J Oper Res*. 2014;235(3):471-483. https://doi.org/10.1016/j.ejor.2013.09.036.
55. Le C, Norato J, Bruns T, Ha C, Tortorelli D. Stress-based topology optimization for continua. *Struct Multidiscip Optim*. 2010;41(4):605-620. https://doi.org/10.1007/s00158-009-0440-y.
56. Holmstr K, Anders OG, Edvall MM. Tomlab Optimization. user' s guide for Tomlab/CONOPT 2007. https://tomopt.com/docs/TOMLAB_CONOPT.pdf.
57. Sigmund O. A 99 line topology optimization code written in matlab. *Struct Multidiscip Optim*. 2001;21(2):120-127. https://doi.org/10.1007/s001580050176.
58. Pedersen CBW. Topology optimization of 2D-frame structures with path-dependent response. *Int J Numer Methods Eng*. 2003;57(10):1471-1501. https://doi.org/10.1002/nme.787.
59. Park C, Kim NH, Haftka RT. The effect of ignoring dependence between failure modes on evaluating system reliability. *Struct Multidiscip Optim*. 2015;52(2):251-268. https://doi.org/10.1007/s00158-015-1239-7.

60. Noh Y, Choi KK, Du L. Reliability-based design optimization of problems with correlated input variables using a Gaussian copula. *Struct Multidiscip Optim*. 2009;38(1):1-16. https://doi.org/10.1007/s00158-008-0277-9.
61. Mathworks. Statistics and machine learning toolbox user's guide 2018a; 2018.

How to cite this article: Shen W, Ohsaki M, Yamakawa M. Robust geometry and topology optimization of plane frames using order statistics and force density method with global stability constraint. *Int J Numer Methods Eng*. 2021;122:3653–3677. https://doi.org/10.1002/nme.6676

APPENDIX A

According to Equations (16) and (17), the confidence level α_k of the first order statistics ($k = 1$) with sample size $m_s = 150$ to approximate the 95% quantile should be 0.9995, which means the probabilities of $\sigma_{1:150}$ and $\gamma_{1:150}$ no less than the corresponding 95% quantiles should be no less than 0.9995. In order to verify this property, a total of 1000 random seeds are used to generate 1000 groups of 150 samples for the uncertainties to investigate the variations of solution R in Example 1 due to difference in sample sets. The mean values, standard deviations, maximum and minimum values of $\sigma_{1:150}$ and $\gamma_{1:150}$ are listed in Table A1. The values of 95% quantiles of σ and γ obtained by Monte Carlo Simulation (MCS) with sample size 1×10^4 are also listed in Table A1. Based on the results of $\sigma_{1:150}$ and $\gamma_{1:150}$ from the 1000 groups of 150 samples, the number of $\sigma_{1:150}$ less than 226.315 MPa is 2 and the number of $\gamma_{1:150}$ less than 0.0904 is 0, indicating that the confidence levels of both of $\sigma_{1:150}$ and $\gamma_{1:150}$ approximating the 95% quantile are greater than 0.9995 for the solution R. Moreover, because the order statistics $\sigma_{1:150}$ and $\gamma_{1:150}$ approximate the extreme quantiles at the tails of the unknown distributions, the mean values of $\sigma_{1:150}$ and $\gamma_{1:150}$ from 1000 groups of 150 samples should be greater than the corresponding 99.3% quantiles using the connection between the order statistics of standard uniform distribution and arbitrary distribution, which is written as

$$\begin{aligned} F_\sigma\left(\frac{1}{1000}\sum_{i=1}^{1000}\sigma_{1:150}^i\right) &\geq \frac{1}{1000}\sum_{i=1}^{1000}F_\sigma(\sigma_{1:150}^i) \approx \overline{\boldsymbol{E}}(F_\sigma(\sigma_{1:150})) = E(U_{1:150}) = 0.993 \\ F_\gamma\left(\frac{1}{1000}\sum_{i=1}^{1000}\gamma_{1:150}^i\right) &\geq \frac{1}{1000}\sum_{i=1}^{1000}F_\gamma(\gamma_{1:150}^i) \approx \overline{\boldsymbol{E}}(F_\gamma(\gamma_{1:150})) = E(U_{1:150}) = 0.993 \end{aligned} \tag{A1}$$

where F_σ and F_γ are the CDF as presented in Equations (16) and (17), and $\overline{\boldsymbol{E}}$ in Equation (A1) represents the expectation operator; $U_{1:150}$ represents the first order statistic of standard uniform distribution with sample size 150. Comparing the results listed in Table A1, it can be seen that the mean values of $\sigma_{1:150}$ and $\gamma_{1:150}$ are all greater than the corresponding 99.3% quantiles, indicating that solution R in Example 1 is able to preserve the robustness of the structure under different sampling sets in statistical sense. Besides, it should be noted that there might be an over-fitting phenomenon if the same uncertainty set is used during optimization procedure, however, the statistical property of solution R of Example 1 indicates that the confidence level is satisfied with difference in sample sets.

Furthermore, in order to investigate the variations of order statistics caused by difference in samples, the following two problems are formulated and solved 10 times for Example 1 with different random seeds in which the first and second order statistics are taken respectively as the objective and global stability constraint functions

TABLE A1 Statistical information of solution R in Example1

Structural response	Mean	Std. dev	Max	Min	95% quantile	99.3% quantile
$\sigma_{1:150}$ (MPa)	247.2407	8.1407	275.7838	223.4451	226.3159	243.1942
$\gamma_{1:150}$	0.09268	8.424×10^{-4}	0.09572	0.09052	0.09041	0.09219

$$\begin{aligned}&\text{Minimize } t\\&\text{subject to } \sigma_{1:150}(\boldsymbol{x}_{\text{free}}(\boldsymbol{q}),\boldsymbol{y}_{\text{free}}(\boldsymbol{q}),\boldsymbol{A};\boldsymbol{\Theta}) \le t;\\&\qquad \gamma^{\text{cr}}_{1:150}(\boldsymbol{x}_{\text{free}}(\boldsymbol{q}),\boldsymbol{y}_{\text{free}}(\boldsymbol{q}),\boldsymbol{A};\boldsymbol{\Theta}) \le \gamma_{\text{U}};\\&\qquad V(\boldsymbol{x}_{\text{free}}(\boldsymbol{q}),\boldsymbol{y}_{\text{free}}(\boldsymbol{q}),\boldsymbol{A}) \le V_{\text{U}};\underline{\boldsymbol{q}} \le \boldsymbol{q} \le \overline{\boldsymbol{q}};\ \ \underline{\boldsymbol{A}} \le \boldsymbol{A} \le \overline{\boldsymbol{A}}\end{aligned} \tag{A2}$$

$$\begin{aligned}&\text{Minimize } t\\&\text{subject to } \sigma_{2:150}(\boldsymbol{x}_{\text{free}}(\boldsymbol{q}),\boldsymbol{y}_{\text{free}}(\boldsymbol{q}),\boldsymbol{A};\boldsymbol{\Theta}) \le t;\\&\qquad \gamma^{\text{cr}}_{2:150}(\boldsymbol{x}_{\text{free}}(\boldsymbol{q}),\boldsymbol{y}_{\text{free}}(\boldsymbol{q}),\boldsymbol{A};\boldsymbol{\Theta}) \le \gamma_{\text{U}};\\&\qquad V(\boldsymbol{x}_{\text{free}}(\boldsymbol{q}),\boldsymbol{y}_{\text{free}}(\boldsymbol{q}),\boldsymbol{A}) \le V_{\text{U}};\underline{\boldsymbol{q}} \le \boldsymbol{q} \le \overline{\boldsymbol{q}};\ \ \underline{\boldsymbol{A}} \le \boldsymbol{A} \le \overline{\boldsymbol{A}}\end{aligned} \tag{A3}$$

The mean values, standard deviations, maximum and minimum values of $\sigma_{1:150}$, $\sigma_{2:150}$, $\gamma_{1:150}$, and $\gamma_{2:150}$ of both problems (A2) and (A3) are listed in Tables A2 and A3, respectively. It can be observed from Table A2 that although $\sigma_{1:150}$ and $\gamma_{1:150}$ vary due to difference in sample sets, their standard deviations are not relatively large compared to the corresponding mean values. The standard deviations of $\sigma_{1:150}$ and $\gamma_{1:150}$ in Table A2 are larger than the standard deviations of $\sigma_{2:150}$ and $\gamma_{2:150}$ in Table A3, however, the ranges between the maximum and minimum values of $\sigma_{1:150}$ and $\gamma_{1:150}$ in Table A2 are smaller than those of $\sigma_{2:150}$ and $\gamma_{2:150}$ in Table A3, indicating that the results obtained by using first order statistics vary in a narrower range due to difference in sample sets, while the results obtained by using second order statistics vary mostly close to the mean values but in a wider range. Moreover, a trade-off relationship is observed such that the mean values and standard deviations of the first order statistics $\sigma_{1:150}$ and $\gamma_{1:150}$ in Table A3 are larger than those of $\sigma_{1:150}$ and $\gamma_{1:150}$listed in Table A2, and similar relationship can be also found by comparing the results of second order statistics $\sigma_{2:150}$ and $\gamma_{2:150}$ in Tables A2 and A3. Therefore, the standard deviation of the extreme order statistics, such as $\sigma_{1:150}$ and $\gamma_{1:150}$, of the final result would be smaller if the extreme order statistics are selected as the objective and constraint functions, while the standard deviation of the non-extreme order statistics of the final result would be smaller than that of extreme order statistics. However, since the extreme order statistics could provide a higher robustness level of the structure where the probability of the structural response not exceeding the extreme order statistics is lower than that of non-extreme order statistics, the extreme order statistics could serve as objective and constraint functions to obtain a structure with prescribed higher robustness level.

TABLE A2 Statistical information of problem (A1) for Example 1

Structural response	Mean	Std. dev	Max	Min
$\sigma_{1:150}$ (MPa)	237.9236	7.6261	252.3201	229.3373
$\gamma_{1:150}$	0.0932	0.001797	0.0943	0.0906
$\sigma_{2:150}$ (MPa)	237.1836	7.1678	252.0981	229.3365
$\gamma_{2:150}$	0.0927	0.001528	0.0942	0.0899

TABLE A3 Statistical information of problem (A2) for Example 1

Structural response	Mean	Std. dev	Max	Min
$\sigma_{1:150}$ (MPa)	245.6271	12.7975	271.7269	234.6596
$\gamma_{1:150}$	0.0989	0.001904	0.1090	0.0948
$\sigma_{2:150}$ (MPa)	227.3847	7.1650	248.0602	220.0783
$\gamma_{2:150}$	0.0985	0.001351	0.1009	0.0943